Hygrothermal aging of a pultruded fiber-polymer composite with predictions for design service lives

Behrouz Zafari[1], J. Toby Mottram[2], Phil Purnell[3], Sotirios Grammatikos[4], Mark Evernden[5]

[1] Dr. Behrouz Zafari, Senior Lecturer, Department of Civil Engineering, Surveying and Construction Management, Kingston University London, London, UK, KT1 2EE. B.Zafari@kingston.ac.uk
[2] Emeritus Professor J. Toby Mottram, School of Engineering, University of Warwick, Coventry, UK, CV4 7AL. Toby.Mottram@warwick.ac.uk
[3] Professor Phil Purnell, School of Civil Engineering, University of Leeds, Leeds, UK, LS2 9LG. p.purnell@leeds.ac.uk
[4] Professor Sotirios Grammatikos, Asemia – Advanced & Sustainable Engineering Materials Laboratory, Department of Manufacturing & Civil Engineering, NTNU - Norwegian University of Science and Technology, 2821 Gjøvik, Norway. sotirios.grammatikos@ntnu.no
[5] Dr. Mark Evernden, Senior Lecturer, Department of Architecture and Civil Engineering, University of Bath, Bath, UK, BA2 7AY. M.Evernden@bath.ac.uk

Corresponding author: b.zafari@kingston.ac.uk

Abstract

This paper presents the findings from an in-depth study, into the influence of hygrothermal aging on material properties of a pultruded flat sheet composite composed of E-CR glass fibers and an unsaturated polyester-based matrix. Through discussing the impact of hygrothermal aging across a total of 10 materials properties, assessing the suitability of test procedures and presenting a framework, to evaluate the suitability of the experimental test results for use with two service life models, this study offers an open and critical evaluation of the currently accepted methods.

Across a total of 102 batches, consisting of 476 coupons, immersed in distilled water at four temperatures of 25, 40, 60 and 80°C, with exposure times varying of 28, 56, 112 and 224 days, the changes in tensile, compressive, in-plane shear and pin-bearing properties are evaluated alongside mass changes. Discussed is an understanding of the relationships obtained for moisture uptake and for material property retentions over time, identifying clearly evidenced non-consistent '*fluctuating trends*'.

The study highlights the possibility of misleading results arising through the impact of forced drying of coupons prior to coupon testing. For longitudinal tensile properties, a direct comparison is made between "Dried" and "Wet" (to represent field conditions) coupons, indicating the need for careful consideration in characterization work for the determination of long-term material properties of composites.

Through the development of a framework for the evaluation of two service life prediction models, the quality of 11 sets of experimental results is evaluated. Using the four most reliable sets predictions of acceleration factors and service lifetimes are reported.

Through evaluation of the experimental findings, testing methodologies and application of service life prediction techniques, this work puts forward an understanding on how to execute experimental programs with accelerated aging with the aim of obtaining meaningful test results for the long-term material properties of fiber-polymer composites.

Keywords: Pultruded fiber-polymer composites; hygrothermal aging; moisture kinetics; material properties; Arrhenius relationship; service life prediction.

Practical Applications

The contribution in this paper to knowledge and understanding on how mechanical properties of fiber-polymer composites might change over time owing to the durability effects of moisture and temperature is important to the determination of adjustment factors for end user conditions, in North American standards and conversion factors for moisture effects and temperature effects in Eurocode standard. These factors are used in structural design codes to adjust the short-term material properties (characteristic values) so that design values of material properties may be appropriate to service lives of fiber-polymer composite structures of, say 50 years.

Introduction

Pultruded fiber-reinforced polymer (PFRP) composites comprise of straight profiles, consisting of a matrix usually based on a thermoset polymer and fiber reinforcement of glass or carbon or hybrid glass and carbon (Bank 2006). Structural PFRP profiles can have the shapes of thin-walled steel profiles (e.g., of I, H, C-channel, and leg-angle shapes), and are exploited in load-bearing structures because of low weight, high durability, and reduced maintenance costs. Such profiles are increasingly used in newbuild bridges, parking garages, railway infrastructure, etc. (Mottram 2011; Mottram and Henderson 2018).

The number of new construction projects using PFRP products might be restricted by a limited understanding of material long-term performance. This hinders confidence in designing PFRP structures for typical service lives of 50 or more years (Karbhari 2007; Mottram and Henderson 2018). Because PFRP profiles do not rust or rot, their durability is potentially superior to comparable steel or timber structural elements. However, the durability and thereby service lives of PFRP structures are affected by several factors, such as the fiber and matrix types, processing parameters, installation and loading conditions, and differences in environmental exposure (Weitsman 1995; Mottram and Henderson 2108). To conduct modeling analysis to predict the long-term behavior of PFRP structures, which can be designed using CEN/TS 19101:2022 (CEN 2022) or ASCE/SEI 74-23 (ASCE 2023), civil engineers require knowledge and understanding on how and why material properties change over time.

Designers face specific challenges in predicting the strengths and stiffnesses of PFRPs as a function of time, environmental conditions, and loading histories (Bank *et al*. 2003; Purnell *et al*. 2008; Ullah *et al*. 2017). The geometrical and chemical complexity of these highly-variable, multi-phase materials, coupled with a lack of published long-term in-service monitoring results, has restricted the development of effective mechanistic models (Bank *et al*. 2003). The most common approach to addressing this challenge has been to use hygrothermal accelerated aging techniques to collect material property by testing within conventional research project time periods (refer to Boinard *et al*. 2000; Correia *et al*. 2006; Cabral-Fonseca *et al*. 2012; Grammatikos *et al*. 2015; Grammatikos *et al*. 2016; Sousa *et al*. 2016; Yang *et al*. 2019; Garrido *et al*. 2022).

The principle of accelerated hygrothermal aging is that data from shorter periods of aging at higher temperatures can be extrapolated to longer periods at lower (i.e., service) temperatures (at which degradation progresses with a slower rate can be quantified cost-effectively, in a reasonable timeframe). To develop appropriate analysis models, we need to consider the temperature dependence of the rate coefficients that govern material property degradation. This is generally done using the Arrhenius relationship:

$$k = k_0 e^{-\frac{E}{RT}} \quad (1)$$

where in Eq. (1), k is the rate constant, k_0 is the reference rate coefficient, E is the molar activation energy for the reaction, R is the universal gas constant, and T is absolute temperature (see also Notation section). Several predictive models have been formulated and presented in attempts to model the lifetime expectancies of degraded (in an accelerated manner) composite materials (White *et al.* 2018). To analytically predict the lifetime by employing Arrhenius-based modeling (Bank *et al*. 2003) is mainly based on the assumption that the age-related degradation of a given material property of a given composite is dominated by a **single** energy-activated physicochemical mechanism, for **all aging** temperatures, up to a limiting temperature (normally taken to be ~20°C below the glass transition temperature, T_g, of the polymer matrix). Above this temperature, physicochemical mechanisms not encountered in the field under service temperatures can dominate, placing a ceiling on the rate of acceleration that may be induced linked to service temperatures. Analysis proceeds by assuming there is a distinct activation energy linked to property changes (Bank *et al*. 2003), and, that a specific fiber degradation mechanism controls strength (Purnell *et al*. 2008). More complex hygrothermal-mechanical multi-phase computational models generally retain an Arrhenius-type relationship at their heart (e.g., Ullah *et al*. 2017), although such models generally do not consider coupling effects (e.g. synergistic coupling of moisture and temperature).

The "Model Specification" approach proposed by Bank *et al*. (2003) has a classification system for mechanical and physical properties of fiber-polymer composites (including PFRPs) employed in construction works. Procedure A provides material acceptance limits based on their "*FRP Material Classification*" in Table A.8.2 and the PFRP material used in this study classifies as "*Glass Type 3*". Procedure B provides a method for predicting long-term material properties. The accelerated aging approach is expected to simulate real aging only when the aging temperatures employed are at least 20°C below the T_g of the characterized coupons. Specimens are subjected to four elevated temperatures, while immersed in distilled water for durations of 28, 56, 112 and 224 days. The testing specification in Bank *et al*. (2003) it is the foundation for the experimental program in the work reported; noting that the material was tested "as received" and so was not fully cured.

The Bank model extends and formalises the well-established Time-Temperature Superposition approach used in polymer physics (e.g. Hiemenz and Lodge 2007). The rate of property loss is assumed to obey a logarithmic relationship; refer to Fig. A.1(a) in A.8.6.9 of Bank *et al*. (2003). The property-time regression line for each temperature must fit sufficiently well, with r^2 (coefficient of determination) > 0.80 for the test results to be deemed valid. If this is established, then a pseudo-Arrhenius plot is constructed with $\log_{10}$(time) on the ordinate axis and "inverse temperature" (1000/K) on the abscissa axis extrapolated out to a constant service temperature for 50, 60, 70 and 80% property retention. This procedure allows for predictions of the service life for a given residual property level and service temperature to be read from the chart (see Fig. A.1(b) in A.8.6.9 of Bank *et al*. 2003). If the data is reliable and robust, a series of parallel lines should result with their slope related to the activation energy (E) of the **single** process that is assumed to dominate degradation. Although not specifically mentioned in Bank *et al.* (2003), E can be determined directly using:

$$E = \frac{AR}{\log_{10} e}, \tag{2}$$

where A is a constant. Note that in Eq. (2) the correction factor for the change of base from 10 to e.

Purnell *et al*. (2008) presented a model to describe hygrothermal aging degradation of polymer composites reinforced with glass fibers (Purnell *et al*. 2006), which was originally developed for glass-fiber reinforced concrete (Purnell *et al*. 2001). The procedure is expressed more explicitly in terms of the Arrhenius parameters of the degradation process by fitting curves, as functions of k and time, derived from micro-mechanical consideration of flaw growth in the glass to strength against time data. Three variants of the general procedure, namely kinetic, diffusion and non-linear were fitted to a range of datasets available in the literature, from both glass-fiber reinforced concrete and glass fiber-polymer composites. A wide range of activation energies (41–118 kJ mol^{-1}) were derived, suggesting that individual materials must be modeled separately (Purnell *et al*. 2008), as dissimilar composites experience different degradations. There was some evidence that datasets with a smaller number of test results produce erroneously low values for their activation energy. The linearity of the derived Arrhenius plots ($1/T$ vs. $\ln(k)$) was extremely high, normally r^2 > 0.95 and the error between mean actual and

136 modelled normalized residual strengths was much less than the typical coefficient of variation in the
137 available test results. Important to the study in this paper is the conclusion by Purnell *et al*. (2008) that
138 "*the diffusion-based simplification of the general model appears to be [most] appropriate, since in the*
139 *general model the non-linear coefficient tends to 0.5; this suggests a diffusion-controlled degradation*
140 *process at the glass surface level*". The modeling procedure is more complex to apply than that for the
141 Bank's model above, while it has the advantage that it is less sensitive to data quality as it effectively
142 combines all the data available rather than considering each time-temperature series separately. Which
143 of these two models is the most appropriate will depend on the data available, the material properties
144 being evaluated and the experience of the analyst.

145 In the Arrhenius relationship of Eq. (1) parameter k_0 in the Purnell *et al*. (2008) model is the rate
146 coefficient for the flaw growth rate. By considering the rate of growth of these flaws, an expression for
147 the residual strength $S(t)$ versus time can be derived as:

148 $$S(t) = \sqrt{\frac{1}{(1+k_0 t)^n}}, \tag{3}$$

149 In Eq. (3) k_0 is symbol k_d in Purnell *et al*. (2008). n relates to the rate of change of growth of flaws, which
150 is usually assumed to be 0.5, yet the modeling process is not very sensitive to the value of n in practice
151 (Purnell *et al*. 2008). Analysis proceeds by least-squares fitting Eq. (3) to each set of reliable strength
152 versus time data derived at different temperatures, and assuming that k_0 is related to T by an Arrhenius-
153 type relationship (via Eq. 1).

154 Plotting $\ln(k_0)$ (ordinate axis) against $1/T$ (abscissa axis) allows the activation energy of the degradation
155 process to be extracted from the slope B of the line, which is $E = BR$. Note that the natural logarithm is
156 used here, not base 10, removing the need to analyse, as necessary in the Bank *et al*. (2003) model, with
157 Eq. (2). No specific requirements are advanced for the quality of the fit of the equations, but in the
158 evaluation r^2 for k_0 against $1/T$ and the root mean square error of the model prediction for $S(t)$, or a
159 similar statistical measure (e.g. a 95% confidence level), should be reported. The most common data
160 quality issue is a failure for the $S(t)$-curve regression to converge, normally because (particularly at lower

ageing temperatures and/or short ageing times) the degree of strength property degradation is less than the inherent variability within the strength data itself. It is of course practical to compute r^2 for the fitted $S(t)$ curves, either individually or as a family, but with this analysis it is not clear what the threshold value should be.

Regardless of the model used, once E has been determined, the acceleration factor, F, can be calculated from Eq. (4) that describes the ratio between a period of in-service time (at a Low Temperature, T_L) equivalent to a given period of accelerated ageing (at a Higher Temperature, T_H):

$$F = \exp\left[\frac{-E}{R}\left(\frac{1}{T_H} - \frac{1}{T_L}\right)\right] \tag{4}$$

In the Bank *et al*. (2003) model, service lifetimes can be read directly from Fig. A.1(b) in A.8.6.9, but for the Purnell *et al*. (2008) model one must set the residual strength $S(t)$ to the desired value (e.g. 0.5 for 50% property retention) in Eq. (3), calculate k_0 for the service temperature of interest from Eq. (1) and solve for time t_{service} using:

$$t_{\text{service}} = \frac{\left[\frac{1}{S(t)^2}\right]^{\frac{1}{n}} + 1}{k_0 \exp\left(\frac{-E}{RT}\right)}. \tag{5}$$

Presented in this paper are test results from an experimental program to characterize 10 material properties using coupons cut from a PFRP ¼ in. (6.4 mm) thick flat sheet. The characterization work is from the three-year UK project DURACOMP (*Providing Confidence in Durable Composites (DURACOMP),* EP/K026925/1), funded by EPSRC, UK. In accordance with the Model Specification from Bank *et al*. (2003) coupons (in batches of five or three (tension only) as defined in Table 1) were subjected to hygrothermal aging by immersion in distilled water at the four temperatures of 25, 40, 60 and 80°C. In Grammatikos *et al*. (2015; 2016) different hygrothermal aged test results from the DURACOMP project have been presented. Reported in this paper is new data for pin-bearing strengths, and the strengths and stiffnesses for in-plane shear, tension, and compression loads.

In contrast to Grammatikos *et al*. (2015), characterization work was conducted with coupons in the wet state, meaning coupon testing happening straight after coupons were removed from the 'hot-wet' aging

environment. These coupons are referred to as "Wet"', meaning the coupons were "*moisture-filled*" owing to a period of aging in distilled water. Previous studies (Grammatikos *et al*. 2015; Sousa *et al*. 2021) have determined material properties after accelerated hygrothermal aging in accordance with ASTM (2014), in which ASTM D5229 specifies the conditioning environment, conditioning time, mass change and mass loss monitoring procedure. This standard requires that coupons be dried to a "*moisture-free*" condition to determine their "*preconditioned mass*"' before conditioning. If the experimental program aims to determine mass losses, then coupons must be "*post-conditioned oven-dry,*" with mass losses measured by subtracting the post-conditioned dry masses from the pre-conditioned dry masses, forcing oven drying to be part of the characterization work. As explained by Grammatikos *et al*. (2020), the consequences of this drying procedure to have "Dried" coupons prior to load testing that determines strengths and/or stiffnesses can be to have two unrealistic effects: 1) it does not represent the actual environmental state after ageing, and 2) it can reverse strength and/or stiffness reductions that are established with "Wet" coupons.

In this work, coupons were weighed and loaded after being dried by using a paper towel to wipe away surface moisture. For strength and stiffness properties of the PFRP material subjected to tension in the Longitudinal direction (i.e., loading aligned with the orientation of unidirectional roving fibers), a comparison is made between the equivalent tensile test results for "post-conditioned oven-dried" or "Dried" coupons, presented in Grammatikos *et al*. (2016), and the "Wet" coupons from this study.

The results of 11 material properties (that excludes the "Dried" Longitudinal tensile modulus of elasticity property), following a data quality check procedure, are analysed using the models introduced above from Bank *et al*. (2003) and Purnell *et al*. (2008). To evaluate the PFRP's suitability for specific applications at a service temperature of 13^{o}C, and a specified design service life (CEN 2002) acceleration factors and life predictions are presented.

Material and Experimental Procedure

The composite material used in this study is the olive-green colored 1500 Series ¼ in. (6.4 mm) thick pultruded flat sheet (FS040.101.096A), manufactured by Creative Pultrusions Inc., Alum Bank, PA

(2016). Its construction is a five-layered lamination, comprising reinforcements of E-CR glass fibers of three Continuous Strand Mat (CSM) layers (nominal total thickness of 2.75 mm) and two unidirectional (UD) roving layers (nominal total thickness of 3.65 mm), which are layers two and four. Fibers are coated with an unknown sizing that forms the interface/interphase region between matrix and fibers that is known to influence property changes due to environmental conditions over time (Mottram and Henderson 2018). The matrix is based on the isophthalic polyester resin Reichhold DION® 31031 (8105M) and has 11 ingredients, involving by mass: 75% of pultrusion resin; 15% of clay filler; 4.5% of styrene and 5.1% for eight minor constituents (for color and processing, etc.). The top and bottom surfaces of the flat sheet material are protected by a thin non-structural polyester veil, which has the dual functions of retarding moisture ingress and shielding the matrix from UV radiation.

The direction of pultrusion, aligned to UD fibers, is referred to as the Longitudinal direction (0^o) and the direction perpendicular is referred to as the Transverse direction (90^o).

Coupons having the required nominal side dimensions specified in Table 1 were cut from 4 ft. (1.22 m) by 8 ft. (2.44 m) flat sheets using a water-cooled diamond saw. The coupons were finished to ±0.05 mm by using a CNC grinding machine to provide exact side dimensions and smooth free edge surfaces. Top and bottom surfaces did not receive any surface preparation.

The resin burn-off method (Ye *et al*. 1995) was used to determine that fiber volume fractions (V_f's) in the UD roving layers was between 55% and 62%, and for the combined mat layers between 24% and 25%, giving an overall fiber volume fraction of 44%. Fig. 1 shows the lay-up after the polymer resin had been burnt off, in which the 'ragged' interfaces indicates that the layer thicknesses of the three CSM layers and two UD layers are not always constant. Taking V_f's of 58 % for rovings and 25 % for mats with mean measured laminae thicknesses and constituent properties, the application of Classical Lamination Theory (CLT) [Bank 2006] permits estimations of the individual lamina elastic constants and estimations of the principal moduli of the PFRP material. The constituent properties were assumed to be: 81 GPa for modulus of elasticity of E-CR-glass fibers (internet source); 0.22 for Poisson's ratio of fibers; 2.6 g/cm^3 for fiber density; 3.2 GPa for the modulus of elasticity of Reichhold DION® 31031 (8105M) polyester

resin (from datasheet); 0.36 for Poisson's ratio of resin; 1.2 g/cm^3 for the density of resin (and matrix). Accordingly, with the assumption of zero porosity, the unaged (benchmark) Longitudinal modulus of elasticity ($E_{L,t}$ (or $E_{L,c}$)) is estimated to be 27.8 GPa (coefficient of variation (CV) is 6% from batch of four resin burn-off samples). The porosity volume fraction was not determined (no air bubbles in the matrix can be seen by visual inspection), yet its presence will have influenced the moisture uptake rate.

Hot-Wet Accelerated Aging

As detailed in Table 1 coupons (of nominal thickness 6.4 mm) were prepared with the following plan dimensions:

(a) 250 by 25 mm for in-plane shear (10^o off-axis) and tension properties;

(b) 70 by 50 mm for compression properties; and

(c) 80 by 80 mm (with a 12 mm semi-circular notch centred on one side) for pin-bearing strengths.

A Setaram Sensys DSC (model no. S60/58367) instrument was used to conduct Differential Scanning Calorimetry measurements to determine T_g. Three unaged samples of PFRP material, without pre-conditioning, were characterized in accordance with standard ISO 11357-2 (ISO 2013) via equal areas analysis with enthalpic recovery. The mean of the cooling and heating T_gs was 105°C. Hence, the maximum hygrothermal aging temperature (80% of T_g) was determined to be 84°C in accordance with the Model Specification (Bank *et al*. 2003), and was the reason for the highest accelerated aging temperature of 80^{o}C.

Without the four edge surfaces being sealed, coupons experienced hygrothermal accelerated aging by immersion in distilled water in thermostatic water baths (Grant, UK) maintained at four different temperatures for a period of 224 days. As seen in Fig. 2, coupons were supported in stainless steel stands to promote a uniform surface exposure.

Moisture uptake

Prior to immersion, batches of five coupons (sizes are given in Table 1) were conditioned in an oven at 30°C for 72 hours to ensure standard dry initial conditions (for “pre-conditioned dry”). Coupons were removed from the water baths at predefined time intervals to weigh water ‘uptake’ in accordance with

the requirements of standard ASTM D5229 (2014), using a digital scale having 0.001g sensitivity. Mass changes ($M(\%)$) were determined using:

$$M(\%) = \frac{M(t)-M(0)}{M(0)} \times 100\% \quad (6)$$

where $M(t)$ and $M(0)$ are mass at zero time and mass as a function of time. Moisture uptake measurements were used to construct gravimetric curves as recommended in the Model Specification.

Fick's second law was employed (assuming uniform moisture and temperature conditions within the body of the coupons) to derive the bulk diffusion coefficient, D, according to the evaluation procedure used in Grammatikos *et al*. (2015). Providing the saturation moisture mass M_∞ can be established from the asymptotic constant equilibrium value of the gravimetric curve, D can be estimated from:

$$D = \pi\left(\frac{h}{4M_\infty}\right)^2\left(\frac{M_2-M_1}{\sqrt{t_2}-\sqrt{t_1}}\right)^2\left(1+\frac{h}{l}+\frac{h}{w}\right)^{-2} \quad (7)$$

where t_1 and t_2 are two aging times on the linear part of the $M(t)$ against t curve, and l, w and h are coupon dimensions of length, width, and thickness. It is assumed that moisture diffusion uptake occurs predominantly in the through-thickness direction, and the dimensional parameter in the last parentheses in Eq. (7) accounts for the contribution to moisture absorption through the edge surfaces (Shen and Springer 1976). Moisture diffusion coefficients were determined only for coupons aged at 60 and 80°C, as to obtain equivalent results at 25 or 40°C would require a significantly extended period of immersion time ($\gg$ 224 days) for coupons to reach moisture saturation M_∞ (also Grammatikos *et al*. 2015).

Mechanical testing

Coupon testing was conducted at room temperature (20±2°C) and 50% relative humidity with loading applied under displacement control (constant rate of 0.01 mm/s), either using a servomotor-driven 100 kN Testometric machines or, for longitudinal compression, under load control using a 400 kN Amsler machine as failure load exceeded 100 kN. Calibration was conducted on both testing machines prior to each series of load tests. A Solartron/ Schlumberger 3531D Orion Delta, TICS International Ltd., UK data logger was employed to record in real time strains (via strain gauges), and their analysis was conducted using MATLAB software.

Figs. 3(a) to 3(c) show the test set-ups for: in-plane shear (10° off axis) and tension loadings; compression loading; and pin-bearing loading, respectively. For the in-plane shear test, the 10° off-axis method was adopted because all the volume of material away from the grips experiences the same shear deformation (Nguyen *et al*. 2018). Other advantages of this method over the standard methods of ISO 15310 (ISO 1999) and ASTM D5379/D5379M (ASTM 2012) are that it is simple to prepare coupons and it does not require special loading fixtures. Experimental determination of the in-plane shear modulus of elasticity, G_{LT}, is challenging as measurement reliability is sensitive to the angle between direction of pultrusion and the loading axis, which must be precisely 10° to the longitudinal axis, which is at 0°. Precision CNC machining was therefore employed to ensure high quality coupons. Surface strains were recorded from a single-side three-element strain gauge Rosette (0°/45°/90°) of type FLAB-5-11 (supplied by Tokyo Sokki Kenkyujo Co., Ltd.), having 5 mm long gauges and G_{LT} was determined from a linear fit of shear stress-shear strain (with $r^2 > 0.99$) generated from the load and gauge readings between 0.05% and 0.25% shear strains.

To determine the Longitudinal tensile strength, $\sigma_{L,t}$, and modulus of elasticity, $E_{L,t}$, testing was conducted on straight coupons (Table 1 and Fig. 3(a)) in accordance with ISO 527-4 (ISO 1997). Aluminium end tabs were bonded using Araldite 2015 epoxy adhesive to prevent premature coupon failure in the gripping region. To record longitudinal strain a FLA -6-11 direct (6 mm) strain gauge was bonded at mid-coupon, with 0° alignment, on one outer surface.

Compression coupon dimensions (Table 1) were tested in accordance with the University of Warwick in-house test method (Mottram, 1994), allowing the coupon width to be 50 mm. Fig. 3(b) shows that the test rig has steel grip fixtures possessing 25 mm deep slots that accommodate the 70 mm long coupons for a gauge length of 20 mm. High quality surface preparation was required to ensure the compressive load is uniformly distributed. The load is transferred mainly via end-bearing with the slots providing lateral restraint that prevent premature end failure and flexural buckling. Uniaxial strain gauges of 1 mm length were bonded at mid-positions and with 0° alignment. For a successful test, the axial strain difference at rupture between the two sides of a coupon is to be < 5% (Mottram 1994).

Pin-bearing strengths were determined using the test procedure reported by Mottram and Zafari (2011), which is now adopted as Procedure C in standard ASTM D953-19 (ASTM 2019). Compression load was applied via a 12 mm diameter fiber-polymer composite rod sitting in a 12 mm semi-circular notch with 0.1 – 0.3 mm clearance (see Fig. 3(c)). The rod was pultruded with UD fiber reinforcement and supplied by Exel Composites (UK) Ltd. The notch was drilled as a hole in a 100 mm high coupon, which then was carefully reamed down to 80 mm using a high precision CNC machine. Pin-bearing strength is calculated by dividing the maximum compression load by the projected area (nominally 76.8 mm^2).

Results and Discussion

Moisture absorption

Plotted in Figs. 4(a) to 4(d) are mean moisture masses, $M(t)$, using Eq. (6) and batches of five coupons, as percentages of the initial dry mass, M_0, against hygrothermal aging time in days. Parts (a) to (d) are for test results to, respectively, characterize coupons for in-plane shear (or tension), longitudinal compression, transverse compression, and pin-bearing. Data points for 15 increasing number of days have symbol of a: 1) circle for 25°C; (2) square for 40°C; (3) diamond for 60°C; and (4) triangle for 80°C. Note that there's substantial mass loss (negative ordinate) at 80°C hygrothermal aging. The initial gradient of these curves (with linearity up to 50 to 60% of maximum moisture uptakes) is used to calculate the rate of moisture uptake and bulk diffusion coefficient (D). Because it is recognized that mass loss commences prior to the saturation point the recorded maximum means can only be representative and are taken as estimations. Using the Gaussian distribution the $M(t)$ data points in Fig, 4 have coefficients of variations typically in the range 5 to 20%, yet can be higher when mass loss dominants at 80°C.

While moisture uptake rate decreases markedly with time at 25°C and 40°C, no coupons at either temperature reached its moisture saturation point after 224 days. Coupons immersed at 60°C are found to have reached M_∞ after approximately 112 days. At 80°C, saturation was reached after approximately 16 days for coupon sized 250 by 25 mm, and 30 days for sizes 70 by 70 mm and 80 by 80 mm coupons, and every 80°C coupon size started to experience a net mass loss between 112 and 140 days.

Plotted in Figs. 5(a) to 5(d) are curves for mean moisture masses (%s) per constant temperature as a function of $\sqrt{t}$, in days. There are four curves per plot that have circle symbols for the in-plane shear coupons (250 × 25 mm), square symbols for pin-bearing coupons (80 × 80 mm), and triangle or diamond symbols for the same-sized coupons (70 × 50 mm) for the Longitudinal and Transverse compression coupons. Note that because the Longitudinal compression coupons have the UD roving reinforcement parallel to the longer side and perpendicular to this side in the Transverse coupons the moisture diffusion is not necessarily identical. Because the side dimensions for the pin-bearing coupons are the same there is no geometrical difference for moisture diffusion between the Longitudinal and Transverse oriented coupons. Therefore, the curves having square symbols shown in Fig. 5 are means from the Transverse batch. The same geometrical condition exists between the in-plane shear and tensile coupons and so in Fig. 5 shows curves having circle symbols for the mean $M(t)$s from the in-plane shear batch of coupons.

Curves in Fig. 5(a) to 5(d) highlight the increase rate of moisture uptake with elevating temperature. The initial rate and the maximum appear to be independent of coupon dimensions, suggesting the orientation of the UD reinforcement did not have a major influence on the diffusion rate. Inspecting the plotted curves there is no discernible difference observed between the mass changes for the Longitudinal and Transverse compression coupons.

Moisture diffusion varies with specimen geometry, as expressed by Eq. (7) over the linear part of the 16 curves. Assuming the plate thickness is constant at 6.4 mm, the nominal ratios for surface area of veil/surface area of edges (Grammatikos *et al*. 2015) and volume/total area for the coupons are calculated to be: 3.6 and 2.5 for in-plane shear; 4.6 and 2.6 for compression; and 6.3 and 2.7 for pin-bearing. Thus, the edge area should be most influential for the in-plane shear coupons and less influential for the pin-bearing coupons. The in-plane shear coupon curves (circle symbol) generally showed the highest rate of uptake; however, the pin-bearing coupon curves (square symbol) did not generally have the lowest absorption rates. At 80°C, when there is significant mass loss, the curves in Fig. 5(d) could be influenced by the ratio of surface area of veil/surface area of edges because the rate of leaching (Grammatikos *et al*. 2015) might be higher from the edge surfaces; this is because the top and bottom

surfaces have a protective veil layer to reduce moisture diffusion. While the mass loss is lower for the pin-bearing coupons (ratio 6.3), the mass loss is similar for the other two coupon sizes (having ratios 4.6 and 3.6). It would appear from the comparison in Fig. 5 that coupon geometry does not have a strong influence on diffusion or mass loss, which conflicts with what was found by Grammatikos *et al*. (2016) when characterizing moisture changes for a significantly bigger specimen of plan size 200 by 200 mm.

Reported in Table 2 are estimations for M_∞ and for D calculated by Eq. (7). It had to be assumed that M_∞ is 'equal' to M_{max} for the coupons aged at 25°C and 40°C despite them not reaching saturation equilibrium after 224 days. Calculations for D's are reported for 60 and 80°C only because coupons had reached moisture saturation (see Figs. 5 and 6). Column (1) in the table is for coupon sizes and the direction for loading relative to the UD alignment for in-plane shear, compression, and pin-bearing testing. Reported in column (2) are M_∞s, as a percentage of M_0 and in column (3) are D values.

Combining the results at 60 and 80°C suggests that M_∞ for the PFRP material is about 1.8 wt%, with the caveat that the effect of mass loss is not included. Assuming 1.8 wt% and using the shape of the $M(t)$ curves for 25°C and 40°C in Figs. 5(a) and 5(b) the M_∞'s in Table 2 are, respectively, estimated to be at least 50% and 11% below saturation values. Moisture changes using the same test procedure and PFRP material are presented in Grammatikos *et al*. (2015) using square coupons that are sized 40 by 40 mm, 80 by 80 mm (same size as the pin-bearing coupons) and 200 by 200 mm. Reported values for M_∞ at 60 and 80°C are in the range 1.8 to 1.9 wt%, except for the smallest specimen size. Grammatikos *et al*. (2015) introduces that at the two higher temperatures significant mass loss ensures maximums can be false. After 224 days Grammatikos *et al*. (2015) recorded a 2 wt% uptake in the smallest specimens and their evaluation indicates that 2 wt% might be close to M_∞ (if there are no active mechanisms for mass loss). This finding indicates that for the PFRP flat sheet the maximum 2 wt% uptake requirement in the Model Specification could be satisfied for this composite being "manufactured properly" (Bank *et al*. 2003).

As expected, D is found to increase with temperature owing to extra thermal energy increasing molecular mobility (Crank 1975). Increasing the temperature from 60°C to 80°C increases the observed rate of

diffusion by 2.8 to 3.8 times, comparable to 2.8 times obtained by Grammatikos *et al*. (2015); i.e., 1.15×10^{-6} mm^2/s at 60°C *c.f.* 3.26×10^{-6} mm^2/s at 80°C.

Non-Fickian behaviour (Bank *et al*. 2003) can be observed in the shape of the 60 and 80°C curves in Figs. 5(c) and 5(d). After the initial, linear stage up to 50 to 60% of the maximum moisture uptake, the rate of diffusion decreases progressively until it reaches the asymptotic constant equilibrium value. It is understood that the unsaturated polyester matrix can only be partially cured by the end of the pultrusion process, and both Surathi and Karbhari (2006) and Roy (2012) have observed that the moisture absorption response is altered when the polymer is not fully cured. This processing condition may lead to a deviation from Fickian behaviour (for a **single** aging mechanism), which is principally caused by polymer relaxation (Berens 1978). After prolonged exposure beyond the equilibrium state, certain polymer entities are known to start losing mass, as observed with the same sheet material by Grammatikos *et al*. (2015) and from the moisture curves in Figs. 5(c) and 5(d). Mass loss is mainly caused by decomposition of the low-molecular weight constituents leading to leaching of species into the water (Morii et al. 1993; Grammatikos *et al*. 2015). It is also understood that a further deviation from Fickian behaviour is induced when aging temperatures are approaching the temperate range for T_g ,as determined via standard test methods (Surathi and Karbhari, 2006). For the scientific reasons to why the curves in Figs. 4(a) to 4(d) show non-Fickian behaviour the authors recommend that caution be taken in the validity of the Fickian derived test results, such as reported in Table 2.

Material Property Test Results

Presented in Tables 3 to 6 are unaged and aged mean material properties, determined using the test batches and procedures introduced above for in-plane shear, tension, compression, and pin-bearing. Means were established from five or three coupons at each temperature/aging time duration. The Coefficient of Variation (CV) for a batch was calculated based on the Gaussian distribution and is given as a percentage in parentheses after the batch mean values. Testing for strength and moduli properties was conducted after periods of 28, 56, 112 and 224 days without allowing the coupons to be “Dried”

(which is the condition specified in ASTM D5229 (ASTM 2014)), and this is why tabulated test results are referred to as "Wet".

Figs. 6 to 10 present batch means as percentage of property retention, which are calculated based on the unaged mean benchmark values. The plotting of results in Figs. 6, 7, 9 and 10 has symbols and straight lines with the same temperature-colors as used in Fig. 4. Symbols are for the positions of the means reported in Tables 3 to 6, with their standard deviations (for assumed Gaussian distribution) shown by 'error bars'. One obvious finding from inspecting the plots is that the variability in the test results for the various material properties is not constant with aging time and/or with the four aging temperatures.

Fig. 8 is specific to the tensile properties, comparing mean test results when the coupons were "Wet" (i.e., in this study) against when coupons are tested "Dried", as reported in Grammatikos *et al*. (2016).

In-plane shear material properties

Presented in Table 3 are "Wet" test results for τ_{LT} and G_{LT}, which are matrix-governed material properties. In order, columns (1) to (4) report aging temperatures, number of aging days, and the τ_{LT}s, and G_{LT}s. Plotted in Figs. 6(a) and 6(b) are the percentage retentions. Respectively, these percentages are based on the mean unaged benchmark values of 35 MPa for τ_{LT} and 3.3 GPa for G_{LT}.

Fig. 6(a) shows that τ_{LT} is reducing by 28 days. For aging at 25°C (circle symbol) and 40°C (square symbol) there follows next a shear strength increases between 28 – 56 days, followed by a slight reduction by 112 days and by 224 days. The overall retention is above 80%. At 60°C (diamond symbol) there is a small reduction to 56 days, no change at 112 days, and then a clear reduction by 224 days, leading to a retention of about 65%. The results at 80°C (triangle symbol) exhibit a continuous reduction in τ_{LT} with the retention at 224 days being about 52% (or 18 MPa).

Fig. 6(b) plots are for G_{LT}. Because the 28-day retentions at the three temperatures of 25, 40 and 80°C are the same at 88% only the triangle symbol for 80°C is seen. G_{LT} at 60°C and 28 days appears to be an outlier because it shows a 6% increase above the benchmark value. Whereas G_{LT} with 80°C aging reduces slightly by 56 days, its value remains constant after 112 and 224 days. For the two lower temperatures the 56-

441 day results are the same as after 28 days at 60°C. By 224 days at 25°C G_{LT} has returned to the benchmark
442 value of 3.3 GPa, whereas at 40°C it is 2.9 GPa, which is also its value after 28 days. At 60°C there is no
443 reduction at 56 days, yet by 224 days retention is 73% or 2.6 GPa this for the lowest mean G_{LT}.

444 When the variation of a material property is found to first decrease or increase, then increase, or
445 decrease, and then decrease or increase the authors are describing this property-time behaviour as
446 having a '*fluctuating trend*'. Such "fluctuating trends" are observed in the 8 plots in Fig. 5.

447 Inspection of the CVs reported in Table 3 shows that they are often < 10% for τ_{LT} and with the mean at
448 6.2% this statistical result signifies an acceptable experimental outcome regarding material variability
449 (Zafari and Mottram 2012). However, for G_{LT} the opposite is observed and because the mean CV at 11.6%
450 is > 10% the quality of the test procedure to determine the in-plane shar modulus is to be questioned;
451 this links back to our understanding from Nguyen *et al*. (2018) that determination of G_{LT} is an
452 experimental challenge.

453 **Tensile material properties**

454 Table 4 reports the "Wet" and "Dried" mean tensile strengths and modulus of elasticities with their
455 percentage CVs, using batches of three coupons. These are fiber-governed material properties. The
456 formatting change in this table is that columns (3) to (6) are for two sets of $\sigma_{L,t}$ and $E_{L,t}$ measurements.
457 Results presented in columns (3) and (5) are extracted from Grammatikos *et al*. (2016), which reports
458 batch means testing "Dried" coupons (in accordance with ASTM D5229 (ASTM 2014)). Only surface
459 wiping for drying was employed before the "Wet" coupons were subjected to tension loading to obtain
460 the means reported in columns (4) and (6). In nearly all other respects the testing methodology for the
461 two test programs was equivalent. However, to avoid direct strain gauge contact with moisture the
462 surfaces where gauges were glued onto "Wet" coupons were precoated with a layer of the two-
463 component room temperature curing polyester PS adhesive, supplied by TML (Tokyo Measuring
464 Instruments Laboratory Co., Ltd.). This precoat created a waterproof layer that permitted the
465 recommended TML CN adhesive to be used to fully bond the gauges to "Wet" coupons in the same manner
466 as they were bonded to "Dried" coupons (Grammatikos *et al*. 2016). The authors' experience has been

467 that without the precoating layer, gauges would not be effectively bonded when coupons are in the "Wet"
468 state. The authors believe that the extra bond layer did not affect the strains measured for the
469 determination of the "Wet" moduli reported in Tables 3 to 5.

470 Fig. 7 is for the retention percentages of "Wet" mean tension properties and has the same plotting format
471 as in Fig. 6. The strength curves in Fig. 7(a), show "*fluctuating trends*" with the number of aging days that
472 can be similar, yet different to "*fluctuating trends*'" seen in the plots in Fig. 6(a) for in-plane shear
473 strength. It is observed that after 224 days the $\sigma_{L,t}$ retention is 69% at 60°C and 52% at 80°C, yet at 25°C
474 and 40°C this strength had increased from the benchmark value of 393 MPa by 7% and 5%.

475 The four curves for the tensile modulus of elasticity presented in Fig. 7(b) highlight, and even more
476 dramatically, a '*fluctuating trend*' at the three temperatures of 25, 40, and 60°C. After 224 days their
477 changes from the benchmark $E_{L,t}$ are -2%, +15% and -8%. The most interesting results are for $E_{L,t}$ at 80°C
478 because not only does this modulus recover with aging time, but after 224 days it is found to be 26%
479 greater than the unaged benchmark mean modulus of 24.5 GPa, listed in Table 4.

480 The resin burn-off method was combined with micromechanical modeling to estimate that $E_{L,t}$ can be in
481 the range 27.0 to 30.3 GPa, for a mean of 27.8 GPa (CV of 6.0%). This semi-empirical treatment indicates
482 that the unaged mean benchmark $E_{L,t}$ at 24.5 GPa can be more representative of a predicted lower
483 characteristic value, at 24.7 GPa, determined from resin burn-off characterization. Based on the
484 micromechanical estimations it is proposed that the characterization work failed to determine a reliable
485 population benchmark mean for $E_{L,t}$ across the 1.22 m (4ft.) width of the flat sheet. The authors offer the
486 following as a plausible scientific explanation for why the "Wet" $E_{L,t}$ can be 31.5 GPa following
487 hygrothermal aging at 80°C for 112 days. There was a greater proportion of UD reinforcement in the
488 "Wet" batch of coupons tested after 112 days than in the equivalent "Wet" batches tested at 0, 28, 56 and
489 224 days. Such batch variations were due to differing proportions of UD reinforcements that is linked to
490 the pultrusion process. The 56-day batch has a mean of 26.1 GPa, which is within the $E_{L,t}$ range derived
491 from tensile testing and resin-burn-off predictions. It is informative that with a CV of 14% (from Table 4)
492 the mean benchmark modulus can have a lower and upper range for characteristic values of 18.9 to 30.1

493 GPa. This relatively broad range in $E_{L,t}$ is for further evidence that within and between batches of three
494 coupons there can be a relatively high variation in the amount of UD roving reinforcement, such that the
495 benchmark mean of 24.5 GPa (reported in Table 4) can be unrepresentative of the population mean.

496 Prior to the DURACOMP project previous characterization work had reported a significant recovery in
497 the modulus of elasticity for the loading types of in-plane shear, tension, and flexure (Karbhari 2007;
498 Sousa *et al*. 2021). One significance different in these studies from the "Wet" results reported in Table 4
499 and Fig. 7 is that the PFRP coupons were tested "Dried"; yet varying fiber distributions in coupon batches
500 could have been a factor. It is, however, understood that relatively small increases in mean moduli can
501 be established after hot-wet aging because of the occurrence of post-curing of partially cured matrices
502 (Surathi and Karbhari; 2006; Roy 2012; Grammatikos *et al*. 2016).

503 To compare the mean tensile properties termed "Wet" (Fig. 7) or "Dried", Fig. 8(a) for $\sigma_{L,t}$ and Fig. 8(b)
504 for $E_{L,t}$ are bar charts with Wet results on right-side and the Dry results on left-side. On the far left side
505 of the bar chart is a darker shaded bar for the benchmark values of 393 MPa and 24.5 GPa. It is evident
506 that for both conditioning states, the means after 224 days at either 25 or 40°C have increased slightly or
507 remained similar to the benchmark means. The influence of the higher aging temperatures of 60 and 80°C
508 in changing the PFRP material properties is evident from inspecting the bar chart results in Figs. 8(a) and
509 8(b).

510 From Fig. 8(a) tensile strength is observed to increase at 25 and 40°C, due to post curing and/or
511 additional crosslinking (with no measurable effect of degradation). At 60 and 80°C, degradation is more
512 pronounced than post curing and thus the strength drops. For "Dried" coupons the reductions in $\sigma_{L,t}$ at
513 224 days (see Fig. 8(a)) are found to be 5% (60°C) and 17% (80°C), respectively. A much more dramatic
514 reduction is witnessed when the coupons stay "Wet" since the percentage reductions for $\sigma_{L,t}$ are
515 considerable at 31% (60°C) and 48% (80°C). This significant difference, with the "Wet" coupons having
516 the greater strength loss, cannot be explained only by known material variabilities, and therefore
517 supports the authors' recommendation that characterization work for the determination of property
518 changes involving moisture diffusion over time should be conducted with the coupons "Wet". The

519 justification for the implementation of this testing procedure is that the "Wet" state more closely
520 represents a state that can be found in the field (Grammatikos *et al*. 2020). It can be concluded that the
521 "Dried" state is solely representing a physical testing state to satisfy a requirement in following standard
522 ASTM D5229 (ASTM 2014).

523 Turning to comparing the "Wet" and "Dried" means for $E_{L,t}$ at 224 days the bar chart in Fig. 8(b) exhibits
524 that this material stiffness is generally higher than the benchmark of 24.5 GPa, except at 60°C. There is
525 no discernible difference between the two conditions. "Wet" $E_{L,t}$ is found to be higher than "Dried" $E_{L,t}$ at
526 40 and 80°C, and *vice versa* at 25 and 60°C. At 80°C and 224 days the increase is 10% for "Dried" coupons
527 and 26% for "Wet" coupons. Post curing and the inherent variation in UD roving reinforcement are two
528 reasons for these observations. For the stiffnesses presented in Fig. 8(b) significant changes owing to
529 aging are not observed, we observe more of the "*fluctuating trend*", which makes it difficult to explain
530 why stiffness drops after drying at 40 and 80°C. Further work will be needed to establish a plausible
531 understanding.

532 Returning to the data reported in Table 4 the CVs provide evidence for the argument that with "Wet"
533 coupons there is less batch variance. Regarding $\sigma_{L,t}$ the mean of the 16 CVs is 9.1% (range 4 to 19%) for
534 "Dried" and 6.5% (range 2 to 12%) for "Wet", with four "Dried" CVs higher than the maximum of 12% for
535 the "Wet" batch at 60°C after 224 days. Similarly, for $E_{L,t}$ the mean of the 16 batch CVs is 8% (range 1 to
536 13%) for "Dried" and 7.4% (range 4 to 10%) for "Wet", with three "Dried" CVs higher than 10% for the
537 two "Wet" batches at 25°C and 56 days and at 60°C and 224 days.

538 **Compressive material properties**

539 Presented in Table 5 are results for "Wet" mean compressive strengths and moduli of elasticities in both
540 Longitudinal and Transverse directions. The table has the same format as in Table 3, now with the
541 Longitudinal properties ($\sigma_{c,L}$ and $E_{L,t}$) in columns (3) and (4), and the Transverse properties ($\sigma_{T,c}$ and $E_{T,t}$)
542 in the columns (5) and (6). Figs. 9(a) to 9(d) are for plots of these means in terms of percentages of
543 retention. In Fig. 9(a) percentages are determined using benchmark $\sigma_{L,c}$ of 377 MPa. Similarly,

benchmark $E_{L,c}$ of 25.9 GPa is used to calculate percentages in Fig. 9(b) and benchmarks of $\sigma_{T,c}$ equal to 148 MPa and $E_{T,c}$ equal to 8.0 GPa are used to construct Figs. 9(c) and 9(d), respectively.

It can be seen from Figs. 9(a) and 9(b) that the variations in $\sigma_{L,c}$ and $E_{L,c}$ are similar in terms of changes observed at individual aging temperatures, yet different in terms of the magnitudes of the changes compared to their tension equivalents $\sigma_{L,t}$ and $E_{L,t}$ displayed in Fig. 7(a) and 7(b). Over the 224 days of the aging changes in $\sigma_{L,c}$ are less than for $\sigma_{L,t}$. $\sigma_{L,c}$ results shows the usual '*fluctuating trends*', which for compressive loading is not as prominent, except at 60°C. The $E_{L,c}$ data points also show '*fluctuating trends*' to 112 days, with the overall change at 224 days less than for $E_{L,t}$. No means reported in Table 4 show that the hygrothermal aging had increased either $\sigma_{L,c}$ or $E_{L,c}$ above their benchmark value. This can be seen as a crucial difference from when the same PFRP material was subjected to tension. There are known differences between the tensile and compressive characterizations. Owing to how compressive force is transferred, compression coupons had double the width of tensile coupons and thereby would have experienced a different moisture uptake. Also, the wider coupon width of 50 mm could have reduced the magnitude of the varying distribution in UD fibers compared to tension coupons at 25 mm wide. Moreover, Longitudinal compressive properties are matrix-governed, whereas Longitudinal tensile properties are fiber-governed.

To indicate acceptable testing for compression properties the "Wet" mean CVs in Table 5 are 8.1% and 7.7% for $\sigma_{L,c}$ and $E_{L,c}$. On average the Longitudinal compression mean CVs are slightly higher than the tension means of 6.5% and 7.4% (from Table 4).

The Transverse compression properties of $\sigma_{T,c}$ and $E_{T,c}$ plotted in Figs. 9(c) and 9(d) show that there is less amplitude in the '*fluctuating trend*' when loading is in the transverse direction, and that the overall retentions after 244 days are lower than for $\sigma_{L,c}$ and $E_{L,c}$, respectively. The four temperature curves for $\sigma_{T,c}$ show a continuing property reduction that has a trend that can be said to be exponentially decaying and no mean exceeds 101% of the benchmarks of $\sigma_{T,c}$ at 148 MPa and $E_{T,c}$ at 8.0 GPa. For the two temperatures of 25 and 40°C the change in stiffness shows an initial decrease by 28 days or at 56 days, respectively, and thereafter $E_{T,c}$ increases. After 224 days the 25°C mean is 8.2 GPa, which is 0.2 GPa

above the unaged benchmark mean, and the 40°C mean is for a 96% retention. In Fig. 9(d) both $E_{T,t}$ curves at 60 and 80°C show a continuous decrease with time. At 5.2% and 6.7% the means of the 16 CVs for $\sigma_{c,L}$ and $E_{L,t}$ are the lowest, showing that the results listed in columns (5) and (6) of Table 5 are reliable.

The Transverse compression strength and modulus retentions at 80°C and 224 days are 34% and 67%, respectively. Results in Tables 4 and 5 offers evidence that after 224 days the deterioration in the Transverse direction is 1.5 times and 2.4 times higher than those in the Longitudinal direction of pultrusion, probably associated with a greater dependence on how the matrix has changed with excessive hot-wet aging (Weitsman 1995).

Pin-bearing strengths

Presented in Table 6 are the "Wet" means of pin-bearing strengths in both Longitudinal and Transverse directions, with the respective CVs. For the convenience of discussing the results, pin-bearing strength is assumed to be a material property, which is a matrix-governed strength. Figs. 10(a) to 10(b) present plots of the two strengths in terms of percentage retention. To establish the percentages, the unaged mean pin-bearing strengths are 304 MPa for $\sigma_{L,br}$ and 213 MPa for $\sigma_{T,br}$.

The characteristics of the four $\sigma_{L,br}$ curves in Fig. 10(a), and to a lesser extent of the four $\sigma_{T,br}$ curves in Fig. 10(b), are observed to be similar to the matrix-governed strength curves for $\sigma_{T,c}$ in Fig. 9(c). There is a tendency for $\sigma_{T,br}$ with time to show a '*fluctuating trend*' that may be present with $\sigma_{L,br}$, and 25°C aging. The other three $\sigma_{L,br}$ curves are for a continuous reduction with aging time. As anticipated, the greatest effect of hygrothermal conditioning occurs at 80°C and after 224 days the strength retention in the Longitudinal and Transverse directions is 63% and 44%, respectively. These two retentions show that for the same moisture uptake of 1.8 wt%, the strength reduction in the Transverse direction is 1.6 times greater than in the Longitudinal direction. This suggests that matrix-governed material properties in the transverse direction could be affected more than in the longitudinal direction, and the technical reason for why is unknown.

At 4.6% and 6.0%, the mean CVs for the two sets of "Wet" pin-bearing strengths are well below 10% (Zafari and Mottram 2012). This finding indicates that the test results are statistically **representative**.

Interpretation of Material Property Test Results

The most striking observation from the test results presented above is that the degree and rate of degradation of material properties with time and temperature of aging varies markedly between the 10 characterized "Wet" material properties. Some properties exhibit smooth, progressive degradation (e.g. $\sigma_{T,c}$), some almost no degradation at all (e.g. $E_{L,c,}$), and other a wide variety of non-smooth Arrhenius type-curve degradations (Eq. 1), leading to the authors describing their responses as having a '*fluctuating trends*'. There is no evidence from the moisture mass results to suggest that different rates of water ingress to the same saturation level can account for this.

The factual information presented in Table 4 and Figs. 7 and 8 is for "Wet" and "Dry" $\sigma_{L,t}$ increases at 25 and 40°C owing to post-curing/additional crosslinking (with no observable effect of degradation). At 60 and 80°C composite degradation is more pronounced than matrix post-curing and thus $\sigma_{L,t}$ reduces. For $E_{L,t}$ the results do not show significant changes owing to aging, which leads to the observed varying '*fluctuating trends*'. It is not straightforward to scientifically explain why tensile stiffness drops at 40 and 80°C, after drying.

In his 1995 review, Weitsman (1995) states that the scientific reason why glassy polymers possess inherent time-dependent behaviours is because their highly complex molecular configurations exist in a non-equilibrium thermodynamic state. Time-dependence is compounded by additional temporal phenomena such as aging, ongoing chemical reactions and post-curing. The time-dependence is accelerated by the fact that absorbed liquids (e.g., moisture) tend to increase the free volume of polymers, thereby lowering their T_g. Weitsman found that typically this reduction in T_g can be by 10°C for each 1 wt% fluid weight uptake in the polymer. About 40% of the mass of the PFRP material is the unsaturated polymer Reichhold DION® 31031 (8105M). A good estimate for M_∞ is 2 wt% of the PFRP mass (accounting for mass loss) and this transforms to 4% for the polymer constituent (neglecting water present in the interphase region), implying that the wet T_g could be between 60 and 70°C. The implication

620 of this observation is that for similar PFRP profiles used outside and exposed continuously, to water the
621 maximum service temperature would be between 40 and 50°C. A corollary from this discussion is that in
622 the Model Specification (Bank *et al*. 2003), the condition T_g – 20°C for the upper limit of aging
623 temperature might require T_g to be defined by a wet T_g and not the dry T_g, which as this characterization
624 work shows, can permit 80°C as an aging temperature.

625 Weitsman (1995) also explains that the increased mobility of the molecular chains and side-groups from
626 the presence of moisture diffusion is denoted as "plasticization". This is essentially a reversible
627 phenomenon, which is why coupons that are "Dried" can possess different material properties to when
628 coupons are load tested in their "Wet" state. This finding has been reported with the comparison of the
629 overall tensile properties presented in Table 7 and in Fig. 8 (for 224 days aging only).

630 The specific behaviour of the PFRP composite at 80 °C (see Figs. 4(a) to 4(d)) can be taken to propose
631 that the overall chemical changes (involving post-curing) and decomposition might have been activated
632 or, alternatively, have been more prominent after a relatively short soaking period (Grammatikos *et al*.
633 2015). This highlights the fact that moisture absorption and chemical changes and decomposition
634 mechanisms are time superimposed. Moreover, it is observed that the moisture absorption process is
635 more prominent in the initial immersion period (at 80°C in the first 10-15 days) and that chemical
636 changes and decomposition are most prominent much later; this understanding is evident from the
637 material properties presented in Table 3 to 6 and Figs. 5 to 10. The authors conclude that for accelerated
638 aging the upper temperature of 80°C was inappropriate, which can result to unrealistic test results and
639 unexpected related material response.

640 The above discussion on the timings of physicochemical changes and decomposition mechanisms within
641 the PFRP coupons subjected to hygrothermal aging leads us to consider the relationship between
642 measured material properties, and the observed '*fluctuating trends*' with aging time. It is observed that
643 the "*fluctuating trends*" in the plots show little consistency between the 10 "Wet" material properties and
644 the four hygrothermal aging temperatures. Combining evidence from the factual discussions on Moisture
645 Absorption and Material Property Test Results, the authors note that the initial state of the PFRP material

was dependent on its post-pultrusion state (i.e. on localized (coupon) variations in proportions of constituents, degree of curing and maybe residual stresses). It is therefore postulate that under hot-wet aging different material states within the PFRP coupons experienced physicochemical mechanisms that acted at different rates and at different times at the four temperatures, and that these mechanisms interacted in a complex way (owing to the current physicochemical state). Should the authors' understanding of physicochemical aging be confirmed for an acceptable interpretation of the test results reported herein the outcome poses a major obstacle to obtaining data from accelerated testing programs with the quality that is required to reliably use predictive models based on the Arrhenius relationship of Eq. (1). This observation is explored further in this paper when the 11 material property datasets are checked for their quality and then analysed using the Bank *et al*. (2003) and Purnell *et al*. (2008) models.

In the context of how structural design standards are dealing with the effects of moisture (and temperature) to establish material properties for design calculations the standard ASCE/SEI 74-23 (ASCE 2023) for the LRFD design of structures of PFRP profiles has for moisture a single adjustment factor to the reference strength value, irrespective of the service temperature. When the matrix is of polyester resin, the adjustment factor is 0.75 for strength and 0.9 for elastic modulus. There is a second adjustment factor, < 1.0 for a constant in-service temperature higher than 32°C, but less than T_g – 22°C, with a limit of 60°C. The Commentary in ASCE/SEI 74-23 (ASCE 2023) explains how these adjustment factors were established.

In accordance with CEN Eurocode Technical Specification CEN/TS 19101 (CEN 2022) the experimental program detailed above is for Exposure Class III, which is for continuous exposure to water (or seawater), permanent immersion in water (or seawater) or permanent exposure to a relative humidity higher than 80% (material temperature up to 25 °C). This most severe Exposure Class for moisture saturation is associated with a Eurocode conversion factor (equivalent to the adjustment factor in ASEC/SEI 74-23) of 0.60 (Garrido *et al*. 2022). This structural design approach denotes that the material properties in limit state formulae shall be reduced to 60% of the short-term (room temperature) characteristic values, to account for the long-term effect of moisture at constant temperature of 20°C (for Class III exposure).

672 Similarly, to the Load and Resistance Factor Design standard, there is a second conversion factor in
673 CEN/TS 19101 (CEN 2022), < 1.0 for a constant service temperature higher than 20°C, limited by T_g –
674 20°C. For additional context, CEN/TS 19101 (CEN 2022) has the conversion factor set to 0.85 (Garrido *et*
675 *al*. 2022) for Exposure Class II, which is for outdoors exposure without: continuous exposure to water;
676 permanent immersion in water; permanent exposure to a relative humidity higher than; and combined
677 UV-radiation and frequent freeze-thaw cycles.

678 The results presented in Tables 3 to 6 confirm that for a service temperature up to 40°C, the LRFD design
679 approach in ASCE (2023) is appropriate for pin-bearing strengths, as well as tension and compression
680 properties, but maybe the adjustment factors should be lower for the in-plane shear properties. In
681 contrast, the Eurocode approach (CEN 2022) with Exposure Class III is observed to be conservative and
682 will be appropriate when the service temperature is increased to 60°C, and this observation includes the
683 in-plane shear properties. For extra context, it is known (Bank *et al*. 2003) that accelerated aging in
684 distilled water is likely to be more aggressive than for other water environments, and is the reason
685 distilled water was the medium for the experimental programme in this paper.

686 Finally, it is clear from an interpretation of the test results, that hygrothermal aging will reduce the
687 strengths of the PFRP material and that long-term retention will be lower when testing coupons that are
688 "Wet". The authors therefore find that it is not advisable to plan for accelerated aging test programs that
689 combines standard ASTM D5229 with material property determination because this route leads to
690 "Dried" coupons for the determination of higher strengths and moduli than can be present in field
691 applications.

692 ## Life Predictions using Bank's and Purnell's Models

693 Outputs from the Bank *et al*. 2003)and Purnell *et al*. 2008 models can be acceleration factors and lifetime
694 predictions using Eqs. (3) and (4). The purpose of the following analyses is to present calculations using
695 these equations. The first analysis stage in using the models is to check the quality of the test results. All
696 the data reported in Tables 3 to 6 for each temperature, time, and property combinations, were checked
697 for their ability to be used in each step of the modeling process.

Three initial (stage 1) checks were made:

Check 1A: Does the data satisfy the requirement of correlation coefficient relationship $r^2 > 0.80$ for the graphical display as per Fig. A.1(a) in A.8.6.9 of the Model Specification (Bank *et al*. 2003)?

Check 1B: Is the slope of the line fitted to the data plotted as in Fig. A.1(a) negative? (A positive slope nominally indicates that the material under analysis is getting stronger (and stiffer) with time, but realistically it is an artefact of the Time-Temperature Superposition approach (Hiemenz and Lodge 2007) and points to 'noisy' and unreliable data.)

Check 1C: Does the data converge when fitting Eq. (3) allowing a value for the first-order rate coefficient k_0 to be derived?

Table 7 reports the results of the stage 1 data quality checking at each of the four temperatures. Temperatures are listed in column (1) and rows three to six report the check results for 10 "Wet" material properties in columns (2) to (11). The eleventh material property in column (12) is for "Dried" $\sigma_{L,t}$. When one of the three checks failed this is indicated by a cell entry in columns (2) to (12) having one or more of *1A*, *IB*, and *1C*. When all three quality checks are passed the cell entry is **X**.

A second quality stage of checking was made on the data transformed according to Model Specification's procedure in Bank *et al*. (2003) for deriving plots equivalent to Fig. 1.A(b) in A.8.6.9. As this combines the results, it is possible that data rejected in the quality stage 1 checks might be suitable if transformed. These stage 2 checks are:

Check 2A: Does the data satisfy the requirement of $r^2 > 0.80$ for plot-type Fig. 1.A(b) in A.8.6.9 of (Bank *et al*. 2003)? (Although a strict reading of Bank *et al*. would suggest that if check *1A* has failed, then plotting graph of Fig. 1.A(b) is irrelevant, yet the authors find there is a degree of ambiguity in the wording and so check *2A* has been included in this analysis.)

Check 2B: Is the slope of the fitted line in plot-type Fig. 1.A(b) positive? (A negative slope would nominally suggest that the material under investigation would last longer at higher temperatures,

but, again, in reality a negative slope identifies that there is 'noisy' data, as for the same outcome in check *1B*.)

The results of the stage 2 checking are given in Table 8 using the same format as in Table 7. For comparison a r^2 value for the Purnell *et al*. (2008) model can also be computed for each family (i.e., with the results from all temperatures combined). r^2s using the Purnell *et al*. (2008) model are reported in the bottom row of Table 8, and there is no limiting value specified.

Table 8 results confirm the narrative that the test results are of variable quality with regards to their analysis by an Arrhenius based model. Datasets in Table 5 for the three tensile properties of $E_{L,t}$, "Wet" $\sigma_{L,t}$ and "Dried" $\sigma_{L,t}$ are found to fail all five quality checks (*1A*, *1B*, *1C*, (Table 7) *2A* and *2B* (Table 8)) at 25 and 40°C, and so these three sets of results are not considered further. Also, the analysis indicates that there is most likely a systematic experimental error involving unrepresentatively weaker coupons for the unaged (or benchmark) characterization of these Longitudinal properties, which the authors believe can be linked to the previously identified variable distribution of UD fiber reinforcement across the 4 ft. (1.22 m) width of the flat sheet, as witnessed in the images of Fig. 1. The remaining eight datasets are in principle all sufficiently robust to be analyzed using the Purnell *et al*. (2008) model procedure, yet further evaluation is needed before those found acceptable will be analysed for life predictions.

The checking procedure for the Purnell *et al*. (2008) model also identifies that several of the datasets are robust enough to be analysed using the Bank *et al*. (2003) model, but choosing which ones is a matter of interpretation. Applying the Bank quality check *A1* strictly would exclude all but the $\sigma_{T,c}$ results from the life-prediction analysis. Interpreting the quality check outcomes more generously to involve checks *2A* and *2B* the data for the three properties $\sigma_{L,c}$, τ_{LT} and $\sigma_{T,br}$ can be included. These four datasets also have r^2 for the Purnell approach at ~0.7; they are given with bold font in the bottom row of Table 8.

It would be feasible to derive an activation energy E for $\sigma_{L,br}$ if the Bank $r^2 > 0.80$ requirement is relaxed, and furthermore for G_{LT} if the data for 25°C aging is also removed from the analysis. However, the uncertainties in the values obtained for E would be very high, as confirmed by the very low r^2 value of 0.07 in the Purnell analysis. The datasets for $E_{L,c}$ and $E_{T,c}$ cannot be modeled with any confidence using

749 either model. Thus, poor-quality datasets have been excluded from an analysis for E and model fit that is
750 presented next.

751 Results for activation energy and statistical data from a Purnell analysis are given in Table 9. Entries in
752 Column (1) are for the four material properties with 'robust' datasets. Columns (2) and (3) are for the
753 calculated -E's and k_0's. The individual r^2s in column (4) refer to the Arrhenius plot of ln(k) against 1/T.
754 This can be compared with the r^2 values calculated for the families of property against time reported in
755 the bottom row of Table 8. It is worth noting that a high r^2 value for the Arrhenius plot does not
756 necessarily correlate with the predictive power of the Purnell *et al*. (2008) model. From Table 8 the mean
757 r^2 for properties $\sigma_{L,c}$, τ_{LT}, $\sigma_{T,c}$, and $\sigma_{T,br}$ is 0.71. This indicates that, on average, the Purnell *et al*. (2008)
758 model accounts for 71% of the variation in the datasets across all four properties. The 95% confidence
759 interval values in column (5) refer to the apparent ability of the k_0 and -E values in columns (2) and (3)
760 to predict the correct value of strength (σ) over the whole range of times (0 to 224 days) and
761 temperatures (25 to 80°C) for a given property.

762 Concerning the Bank model, E directly calculated using Eq. (2) in the Model Specification method (Bank
763 *et al*. 2003) for the only fully compatible data of $\sigma_{T,c}$ is 58.0 kJ/mol, with the 95% confidence level at ±3.7
764 kJ/mol. With the Purnell analysis the E value of 56.9 kJ/mol is for a good agreement. For the other three
765 datasets of potentially adequate quality the calculated Es are: 107.9 kJ/mol for $\sigma_{L,c}$ (with 95% confidence
766 level at ±76.7 kJ/mol), 53.5 kJ/mol for τ_{LT} (with 95% confidence level at ±38.9 kJ/mol), and 78.0 kJ/mol
767 for $\sigma_{T,br}$ (with 95% confidence level at ±49.6 kJ/mol). Comparing with the Es in Table 8 from the Purnell
768 analysis the same rank order is observed, yet it is noted that the large uncertainties are derived from the
769 average of the values of the slopes of the 50, 60, 70 and 80% property retention lines from plotted test
770 results, as per Fig. 1.A(b) of A.8.6.9 in Bank *et al*. (2003).

771 Computing the family and overall r^2s from the Bank *et al*. (2003) modelling is not straightforward and
772 must be done iteratively. First, an average slope of the quasi-parallel lines on graph-type Fig. 1.A(b) for
773 $\log_{10}$(time) against 1000/T must be found. Then, a least-squares regression must be performed for each
774 material property retention line with the slope set to the average to determine the appropriate value for

the intercept. The resultant values of slope and intercept for the various property retention levels may next be used to reconstitute the property retention against time curves for each material property to be compared with the test results. Applying this analysis procedure gives r^2 of 0.64 for Transverse compressive strength (the most robust dataset), but low or negative r^2s for other three robust properties. This latter finding means the analysis procedure presented in Bank *et al*. (2003) is unable to reliably account for the variation in the experimental results, other than for $\sigma_{T,c}$.

Predictions of activation energies from both models are comparable, both in terms of magnitude and variability with those previously reported for glass fiber-polymer composites (e.g. 41-90 kJ/mol (Purnell *et al*. 2008), 48-51 kJ/mol (Li *et al*. 2018), 38-54 kJ/mol (Krauklis *et al*. 2022), 14-46 kJ/mol (Hota *et al*. 2020)). The wide range of *E*s reported here and elsewhere indicates that there is a variety of physiochemical processes responsible for aging mechanisms that depend on the specific composite material and material property under study, rather than on one or two physicochemical mechanisms dominating aging in general.

Using the analysis values presented in Table 9, it is practical to use Eq. (4) to calculate acceleration factors. These are presented in Table 10 for service temperatures of 13°C (reflecting an average annual outdoor exposure at New York, New York State, USA or London, UK, cities) and 18°C (reflecting PFRP structure located in Los Angeles, California, USA or Buenos Aires, Argentina cities), and ageing temperatures of 40, 50, 60 and 80°C. It is observed that there is a wide range in the predicted acceleration factors with lowest range of 2.4 to 11 for the in-plane shear strength and highest range of 5.2 to 94 for Transverse compression strength.

Thus, for an expected 50-year design service life, depending on the material property controlling failure the mean required accelerated ageing time to detect a rupture-type failure could be between 6 months (for degradation of Transverse compressive strength in London if subjected to hygrothermal testing at 80°C) or 21 years (for degradation of in-plane shear strength in Los Angeles similar tested continuously at 40°C). These predictions are to highlight the need for researchers to design hygrothermal ageing programs carefully, see also final paragraph on Interpretation of Material Property Test Results, to have

confidence that the test results could be of the quality to pass the stage 1 and stage 2 checks presented above.

Service lifetimes can also be predicted from the data by employing Eq. (5) for $t_{service}$. Presented in Table 11 are examples for a service temperature of 13°C and four property retention thresholds from 40 to 70%. It is encouraging to observe that at 40% retention, which is for a stress level exceeding sustained design load cases for the PFRP flat sheet plate material (CEN 2022; ASCE 2023), the lowest service lifetime is 44 years. Furthermore, the $t_{service}$ predictions reported in Table 11 clearly show that if sustained stress levels are 50% or higher the detrimental effect of hygrothermal aging on material properties of the PFRP would preclude this material from being used in structural engineering applications.

Concluding Remarks

The findings from this research work can be summarized as follows:

- Characterization work with an 'off-the-shelf' pultruded flat sheet composite has generated 10 datasets of experimental results to show how different material properties change with accelerated aging in distilled water over 224 days, and at four temperatures between 25 to 80°C.
- For the 6.4 mm (1/4 in.) thick laminate the maximum moisture mass uptake (with non-Fickian behaviour) is estimated to be 2 wt%; the true maximum is unknown because moisture absorption is accompanied with mass loss owing to matrix degradation.
- 2 wt% of additional water inside the fiber-polymer composite could equate to a reduction in the glass transition temperature of 40°C, and this suggests that the maximum service temperature for this pultrusion product could be 50 to 60°C.
- Evaluation of the test results shows that accelerated aging cannot be conducted at 80°C, which is a temperature satisfying the condition of the dry glass transition temperature minus 20°C. The authors recommend that the maximum aging temperature in accelerated aging testing should be limited to the "Wet" glass transition temperature, which for pultruded material could be closer to 60°C for a moisture mass increase of 2 wt%.

827 • Without coupon pre-drying, the 40 plotted curves for mean batch properties of 10 "Wet" material
828 properties show that no property varies over 224 days in a manner that is for a single dominant
829 mechanism of degradation. In fact, the plotted data often shows non-consistent '*fluctuating*
830 *trends'*.
831 • Scientific reasons for measured properties to be greater than their unaged (benchmark) values
832 can be post-curing and a non-uniform distribution of undirectional roving fibers across the 1.22
833 m (4 ft.) width of the flat sheet. A corollary from the latter reason is that every batch of aged
834 coupons should have had an unaged batch to ensure that relevant benchmark properties were
835 available to know precise batch changes.
836 • The non-consistency in the '*fluctuating trends*' has led the authors and Grammatikos *et al*. (2016)
837 to postulate that the flat sheet material, under hot-wet aging, experienced a number of
838 physicochemical mechanisms that acted at different rates and different times at the four constant
839 temperatures, and which interacted in a complex way owing to the current physicochemical state
840 of the material that is continuously changing the material properties.
841 • This material response owing to moisture diffusion over time is for an understanding that
842 accelerated aging cannot be easily employed to characterize property changes experienced by
843 composite structures in the field.
844 • After 224 days of hot-wet aging all properties had reduced below the unaged values when the
845 temperature is 60^{o}C or higher, which signifies that the degradation mechanisms, such as matrix
846 decomposition, superseded any strengthening mechanisms such as additional post-curing, which
847 are more prominent in the early phase of aging.
848 • The tension strengths and modulus of elasticities determined with "Wet" and "Dried" (for coupon
849 testing in accordance with ASTM D5229 (ASTM 2014)) coupons are compared to establish that
850 retention percentages were significantly higher, by over 25% for the "Dried" batches. The authors
851 therefore cannot recommend coupon drying as being part of an accelerated aging test program
852 and the justification for this understanding is that by drying coupons prior to load testing the

composite's state is less representative of field conditions and this can lead to characterizing properties that are too high.

- By comparing the retention percentages of materials properties after 224 days of aging with how structural design guidance (ASCE 2023, CEN 2022) scope the reduction in the value of characteristic values due to long-term moisture absorption it is observed that their approaches should be acceptable.
- An analysis has been performed using models based on the Arrhenius relationship that assumes a single mechanism is causing aging degradation that can be identified by reductions of material properties. Five checks conducted, in two stages, on 11 datasets (10 "Wet" and one "Dry") establishes that the overall quality of data for this analysis is low. This finding can have a direct link to the non-consistent '*fluctuating trends*', complex relationships of competing physicochemical mechanisms and the non-uniform unidirectional fiber distribution across the flat sheet's width.
- Analysing four material properties that passed several of the dataset checks gave acceleration factors in the range of 2.4 to 11 for the in-plane shear strength and 5.2 to 94 for transverse compression strength. Different physicochemical mechanisms over time could be controlling these measured differences.
- For a service temperature of 13^{o}C, the analysis predicts that for a 40% strength retention the lowest service lifetime is 44 years. This is an encouraging finding because this level of stress will exceed the sustained (long-term) stress that this pultruded composite could experience in the field, following structural design calculations to ASCE (2023) or CEN (2022).
- Finally, the findings from the characterization work of the DURACOMP project can support the planning of future experimental programs with accelerated aging to obtain test results that can be analysed by the appropriate modeling to obtain useful predictions for the service live strengths of fiber-polymer composites.

Data Availability Statement

879 All data, models, and code generated or used during the study appear in the submitted article.

880 **Acknowledgments**

881 The work was conducted as part of the research program with the EPSRC funded project DURACOMP
882 (*Providing Confidence in Durable Composites*, EP/K026925/1). The authors acknowledge that the test
883 results presented could not have been generated without professional service support from the
884 engineering technicians within the School of Engineering at The University of Warwick.

885 **Notation**

886 *The following symbols are used in this paper*:

887 A = constant;

888 B = slope;

889 e = 2.718281828;

890 D = bulk diffusion coefficient;

891 E = molar activation energy for the reaction;

892 $E_{L,t}$ = Longitudinal tensile modulus of elasticity;

893 $E_{L,c}$ = Longitudinal compressive modulus of elasticity;

894 $E_{T,t}$ = Transverse tensile modulus of elasticity;

895 $E_{T,c}$ = Transverse compressive modulus of elasticity;

896 G_{LT} = in-plane shear modulus of elasticity;

897 h = thickness;

898 k = rate constant;

899 k_0 = reference rate coefficient or rate coefficient for the flaw growth rate (Purnell *et al*. (2008)
900 model);

901 l = length;

902 M = mass;

903 M_1 = mass at time t_1;

904 M_2 = mass at time t_2;

905 $M(t)$ = mass as a function of time;

906 $M(0)$ = mass at zero time;

907 M_∞ = mass at time infinity;

908 n = parameter related to the rate of change of growth of flaws;

909 r^2 = coefficient of determination;

910 R = universal gas constant;

911 $S(t)$ = residual strength;

912 t = time;

913 $t_{service}$ = service time;

914 t_1 = time at point 1;

915 t_2 = time at point 2;

916 T = absolute temperature;

917 T_g = glass transition temperature;

918 T_H = High temperature;

919 T_L = Low temperature;

920 w = width;

921 $\sigma_{L,br}$ = Longitudinal pin-bearing strength;

922 $\sigma_{L,c}$ = Longitudinal compressive strength;

923 $\sigma_{L,t}$ = Longitudinal tensile strength;

924 $\sigma_{T,br}$ = Transverse pin-bearing strength;

925 $\sigma_{T,c}$ = Transverse compressive strength;

926 τ_{LT} = in-plane shear strength.

927 **References**

928 ASCE 2023. *Standard for load and resistance factor design (LRFD) of pultruded fiber reinforced polymer*
929 *(FRP) structures*, ASCE/SEI 74-23, Reston, VA: American Society of Civil Engineers and Structural
930 Engineering Institute.

931 ASTM 2012. *Standard test method for shear properties of composite materials by the V-notched beam*
932 *method.* ASTM D5379/D5379M-12. West Conshohocken, PA: American Society of Testing and Materials
933 (ASTM).
934 ASTM 2014. *Standard test method for moisture absorption properties and equilibrium conditioning of*
935 *polymer matrix composite materials*. ASTM D5229. West Conshohocken, PA: American Society of Testing
936 and Materials (ASTM).
937 ASTM 2019. *Standard test method for pin-bearing strength of plastics*. ASTM D953-19. West
938 Conshohocken, PA: American Society of Testing and Materials (ASTM).
939 Bank L. C. 2006. *Composites for construction: Structural design with FRP materials*. John Wiley & Sons.
940 Berens, A. R. 1978. "Analysis of transport behavior in polymer powders." *J. Membr. Sci.* 3 (2): 247-264.
941 https://doi.org/10.1016/S0376-7388(00)83025-2
942 Boinard, R., Pethrick, R. A., Dalzel-Job, J. and Macfarlane, C .J. 2000. "Influence of resin chemistry on water
943 uptake and environmental ageing in glass fibre reinforced composites-polyester and vinyl ester
944 laminates." *J. Mat. Sci.* 35;1931-1937. https://doi.org/10.1023/A:1004766418966
945 Bank, L. C., Gentry T. R, Thompson, B. P. and Russell, J. S. 2003. "A model specification for FRP composites
946 for civil engineering structures." *Constr. Build. Mater.* 17(6-7): 405-437.
947 https://doi.org/10.1016/S0950-0618(03)00041-2
948 Cabral-Fonseca, S., Correia, J. R., Rodrigues, M. P. and Branco, F.A. 2012. "Artificial accelerated ageing of
949 GFRP pultruded profiles made of polyester and vinylester resins: Characterisation of physical–chemical
950 and mechanical damage." *Strain* 48: 162-173. https://doi.org/10.1111/j.1475-1305.2011.00810.x
951 CEN 2002. *Eurocode 0 - Basis of structural design*. EN 1990. Brussels, Belgium: European Committee for
952 Standardization.
953 CEN 2022. *Design of fibre-polymer composite structures*. CEN/TC 250. Brussels, Belgium: European
954 Committee for Standardization.
955 Correia, J. R., Cabral-Fonseca, S., Branco, F. A., Ferreira, J. G., Eusebio, M. I. and Rodrigues, M. P. 2006.
956 "Durability of pultruded glass-fiber-reinforced polyester profiles for structural applications," *Mech.*
957 *Compos. Mater.* 42 (4): 325–338. https://doi.org/10.1007/s11029-006-0042-3

Crank, J. 1975. *The mathematics of diffusion*. Oxford, England: Clarendon Press.

Creative Pultrusions, Inc. (2016), *The new and improved Pultex® pultrusion design manual (imperial version)*. Alum Bank, PA: Creative Pultrusions, Inc.

Garrido, M., J. M. Sousa, J. R. Correia, and Cabral-Fonseca, S., 2022. "Prediction of long-term performance and definition of a moisture conversion factor for the durability design of pultruded GFRP profiles under hygrothermal exposure." *Constr. Build. Mater.* 326: 126856. https://doi.org/10.1016/j.conbuildmat.2022.126856

Grammatikos S. A., Zafari B., Evernden M. C., Mottram J. T. and Mitchels J. M. 2015. "Moisture uptake characteristics of a pultruded fibre reinforced polymer flat sheet subjected to hot/wet aging." *Poly. Degrade. and Stab.* 121: 407-419. https://doi.org/10.1016/j.polymdegradstab.2015.10.001

Grammatikos, S. A., Evernden, M., Mitchels, J., Zafari, B., Mottram, J. T. and Papanicolaou, G. C. 2016. "On the response to hygrothermal aging of pultruded FRPs used in the civil engineering sector." *Mater. Des*. 96: 283-295. https://doi.org/10.1016/j.matdes.2016.02.026

Grammatikos, S., Papatzani, S., Evernden, M. 2020. "Is hygrothermal aging of construction polymer composites a reversible process?" in *Proceedings of IOP Conference Series: Materials Science and Engineering*, IOP Publishing, Vol. 842 No. 1, 012004. https://doi.org/10.1088/1757-899X/842/1/012004

Hiemenz, P. C. and Lodge, T. P. 2007. *Polymer Chemistry*, 2nd Edition. Boca Raton, FL: Taylor & Francis.

ISO 1997. *Plastics - Determination of tensile properties Part 4: Test conditions for isotropic and orthotropic fibre-reinforced plastic composites*. ISO 527-4. Geneva, Switzerland: International Organization for Standardization.

Hota, G., Barker, W. and Manalo, A. 2020. "Degradation mechanism of glass fiber/vinylester-based composite materials under accelerated and natural aging." *Constr. Build. Mater.* 256: 119642. https://doi.org/10.1016/j.conbuildmat.2020.119462

ISO 1999. *Fibre-reinforced plastic composites-determination of the in-plane shear modulus by the plate twist method*. ISO 15310. Geneva, Switzerland: International Organization for Standardization.

ISO 2013. *Plastics Differential scanning calorimetry (DSC) Part 2: Determination of glass transition temperature and step height*. ISO 11357-2. Geneva, Switzerland: International Organization for Standardization.

Karbhari, V. M. 2007. *Durability of composites for civil structural applications*. Cambridge, UK: Woodhead Publishing and Institute of Materials, Minerals and Mining (IOM^3).

Krauklis, A. E., Aouissi, H. A., Bencedira, S., Urlakovs, J., Zekker, I., Bute, I. and Klavins, M. 2022. "Influence of environmental parameters and fiber orientation on dissolution kinetics of glass fibers in polymer composites." *J. Compos. Sci.* 6 (7): 210-237. https://doi.org/10.3390/jcs6070210

Li, R., Ye, L. and Li, G., "Long-term hydrothermal aging behavior and aging mechanism of glass fibre reinforced polyamide 6 composites." *J. Macromol. Sci.* Part B 57 (2): 67-82. https://doi.org/10.1080/00222348.2018.1432174

Morii, T., Tanimoto, T., Hamada, H., Maekawa, Z-I., Hirano, T. and Kiyosumi, K., 1993. "Weight changes of a randomly orientated GRP panel in hot water." *Compos. Sci. Tech.* 49(3): 209-216. https://doi.org/10.1016/0266-3538(93)90103-N

Mottram, J. T., 1994. "Compression strength of pultruded flat sheet material," *J. Mater. Civ. Engrg.* 6 (2), 185-200. https://doi.org/10.1061/(ASCE)0899-1561(1994)6:2(185)

Mottram, J. T. 2011. "Does performance based design with fibre reinforced polymer components and structures provide any new benefits and challenges?" *Struct. Engr.*, 89 (6): 23-27.

Mottram, J. T. and Henderson, J. (Eds.). 2018. *FRP Bridges – Guidance for Designers.* CIRIA C779. London.

Mottram, J. T. and Zafari, B. 2011. "Pin-bearing strengths for design of bolted connections in pultruded structures." *P. I. Civil Eng-Str. B.,* 164 (SB5): 291-305. https://doi.org/10.1680/stbu.2011.164.5.291

Zafari, B. and Mottram, J. T. 2012. "Effect of hot-wet aging on the pin-bearing strength of a pultruded material with polyester matrix," *J. Compos. Constr*., 16(3): 340-352. https://doi.org/10.1061/(ASCE)CC.1943-5614.0000258

Nguyen, T. T., Chan, T. M. and Mottram, J. T. 2018. "Reliable in-plane shear modulus for pultruded FRP shapes," *P. I. Civil Eng-Str. B.* 171 (11): 818-829. https://doi.org/10.1680/jstbu.16.00194

1010 Purnell, P., Short, N. R. and Page, C. L. 2001. "A static fatigue model for the durability of glass fibre
1011 reinforced cement," *J. Mater. Sci.* 36: 5385-5390. https://doi.org/10.1023/A:1012496625210
1012 Purnell, P., Lesko, J. and Cain J. 2006. "Accelerated ageing rationales for GRC and their application to GRP."
1013 *In Proceedings of Conference DURACOSYS: Durability of Composite Systems*, Virginia Tech., Blacksburg. VA.
1014 Purnell, P., Cain, J., Van Itterbeeck, P. and Lesko, J. 2008. "Service life modelling of fibre composites: A
1015 unified approach." *Compos. Sci. Technol.* 68 (15-16): 3330-3336.
1016 https://doi.org/10.1016/j.compscitech.2008.08.026
1017 Shen, C-H. and Springer, G.S. 1976. "Moisture absorption and desorption of composite materials." *Compos.*
1018 *Mater.* 10 (1):2-20. https://doi.org/10.1177/002199837601000101
1019 Sousa, J. M., Correia, J. R. and Cabral-Fonseca, S. 2016. "Durability of glass fibre reinforced polymer
1020 pultruded profiles: Comparison between QUV accelerated exposure and natural weathering in a
1021 mediterranean climate." *Exp. Tech.* 40 (1): 207–219. https://doi.org/10.1007/s40799-016-0024-x
1022 Sousa, J. M., Garrido, M., Correia, J. R. and Cabral-Fonseca, S. 2021. "Hygrothermal ageing of pultruded
1023 GFRP profiles: Comparative study of unsaturated polyester and vinyl ester resin matrices." *Compos. Part*
1024 *A Appl. Sci. Manuf.*, 140: 106193. https://doi.org/10.1016/j.compositesa.2020.106193
1025 Surathi, P. and Karbhari, V. M. 2006. *Hygrothermal effects on durability and moisture kinetics of fiber-*
1026 *reinforced polymer composites.* Report No. FHWA/CA/ES-07/01. Sacramento, CA: California Department
1027 of Transportation. Division of Engineering Service.
1028 Roy, S. 2012. Moisture-induced degradation, 181-236. Chapter 6 in: K. V. Pochiraju, G. P. Tandon, G. A.
1029 Schoeppner (Eds.), *Long-term durability of polymeric matrix composites.* New York, NY: Springer.
1030 Ullah, Z., Kaczmarczyk, Ł, Grammatikos, S. A., Evernden, M. C. and Pearce C. J. 2017. "Multi-scale
1031 computational homogenisation to predict the long-term durability of composite structures." *Compos.*
1032 *Struct.* 181: 21-31. https://doi.org/10.1016/j.compstruc.2016.11.002
1033 Weitsman, Y. J. 1995. *Effect of fluids on polymeric composites-A review*. Report MAES 95-1.0 CM, Arlington,
1034 VA: Office of Naval Research.
1035 White, C. C., White, K. M. and Pickett, J. E. (Ed.). 2018. *Service life prediction of polymers and plastics*
1036 *Exposed to outdoor weathering*, A volume in Plastics Design Library, William Andrew Publishing, Oxford.

Yang, S., Liu, W., Fang, Y. and Huo, R. 2019. "Influence of hygrothermal aging on the durability and interfacial performance of pultruded glass." *J. Mater. Sci.* 54 :2102–2121. https://doi.org/10.1007/s10853-018-2944-6

Ye, B. S., Svenson, A. L. and Bank, L. C. 1995 "Mass and volume fraction properties of pultruded glass fibre-reinforced composites," *Compos.* 26 (10): 725-731. https://doi.org/10.1016/0010-4361(95)91140-Z

Table Captions

Table 1. Defining coupons, constant aging temperatures and immersion times in days.

Table 2. Maximum moisture masses and diffusion coefficients.

Table 3. Test results for mean in-plane shear strengths and in-plane shear moduli with coefficients of variation (in backets).

Table 4. Test results for mean Longitudinal tensile strengths and tensile modulus of elasticities with coefficients of variation (in backets).

Table 5. Test results for mean Longitudinal and Transverse compression strengths and modulus of elasticities with coefficients of variations (in backets).

Table 6. Test results for mean Longitudinal and Transvers bearing strengths with coefficients of variation (in backets).

Table 7. Data quality stage 1 checks.

Table 8. Data quality check Sage 2 checks.

Table 9. Activation energy and statistical data for the Purnell analysis.

Table 10. Acceleration factors, *F*, from using Eq. (4).

Table 11. Mean service lifetimes ($t_{service}$ in years) at 13°C for each property at various retention levels.

Figure Captions

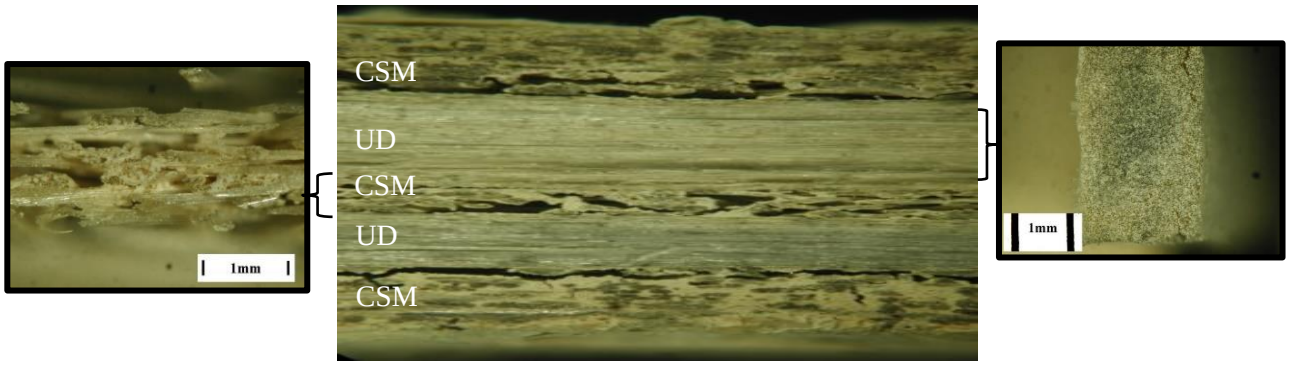

Fig. 1. Lamina lay-up for the flat sheet PFRP material (FS040.101.096A).

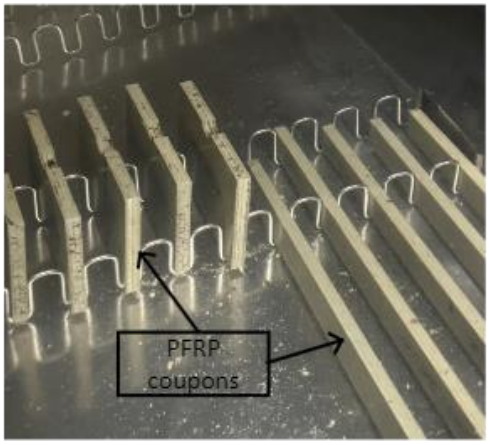

Fig. 2. Coupons immersed in a water tank for hygrothermal aging.

(a) (b) (c)

Fig. 3. Test set-ups: a) 10° off axis in-plane shear (and tension); b) Compression; c) Pin-bearing.

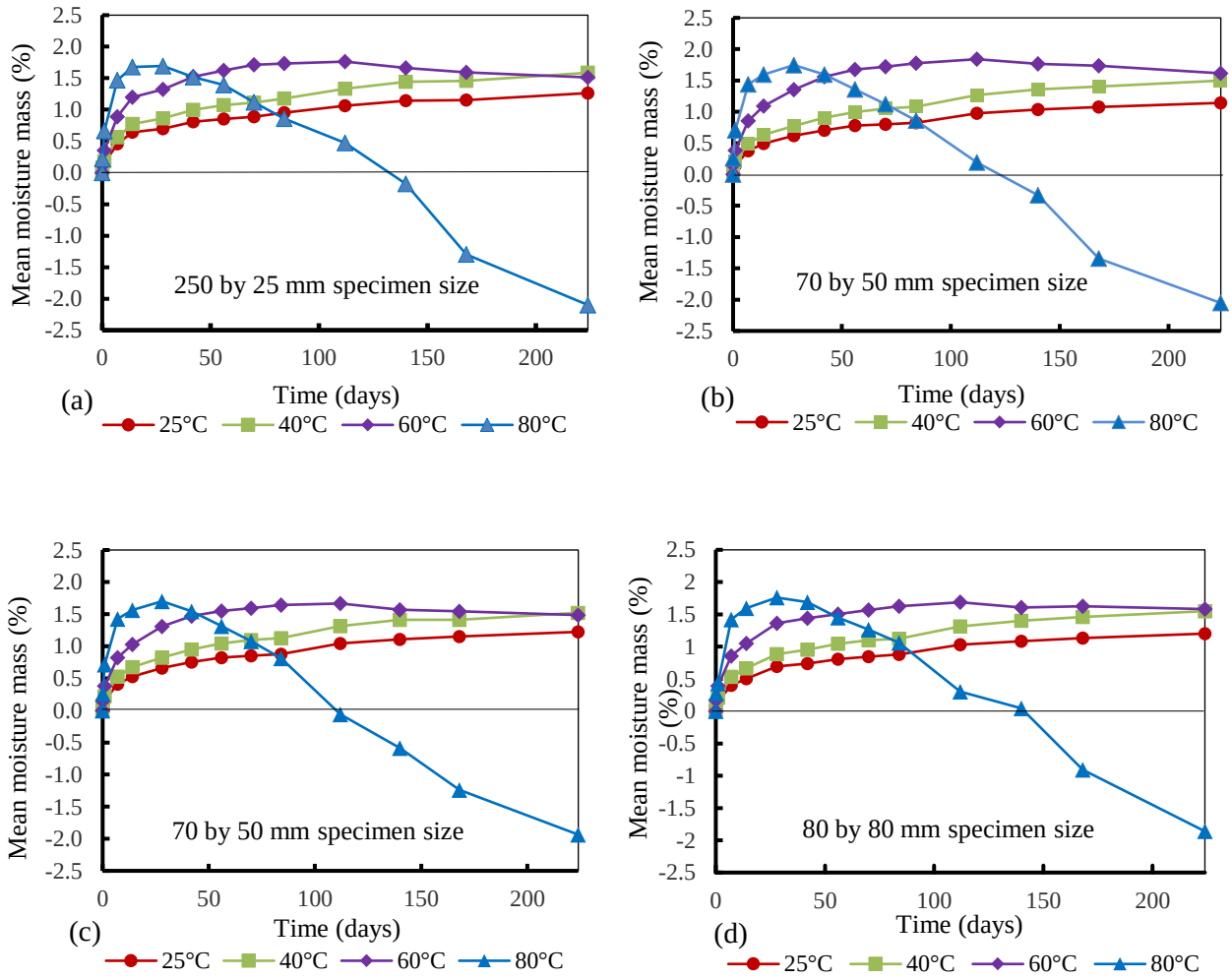

Fig. 4. Mean moisture mass (%) curves with time (in days) at four temperatures and for coupon sizes of: (a) 250 by 25 mm (in-plane shear); (b) and (c) 70 by 50 mm (compression); (d) 80 by 80 mm (pin-bearing).

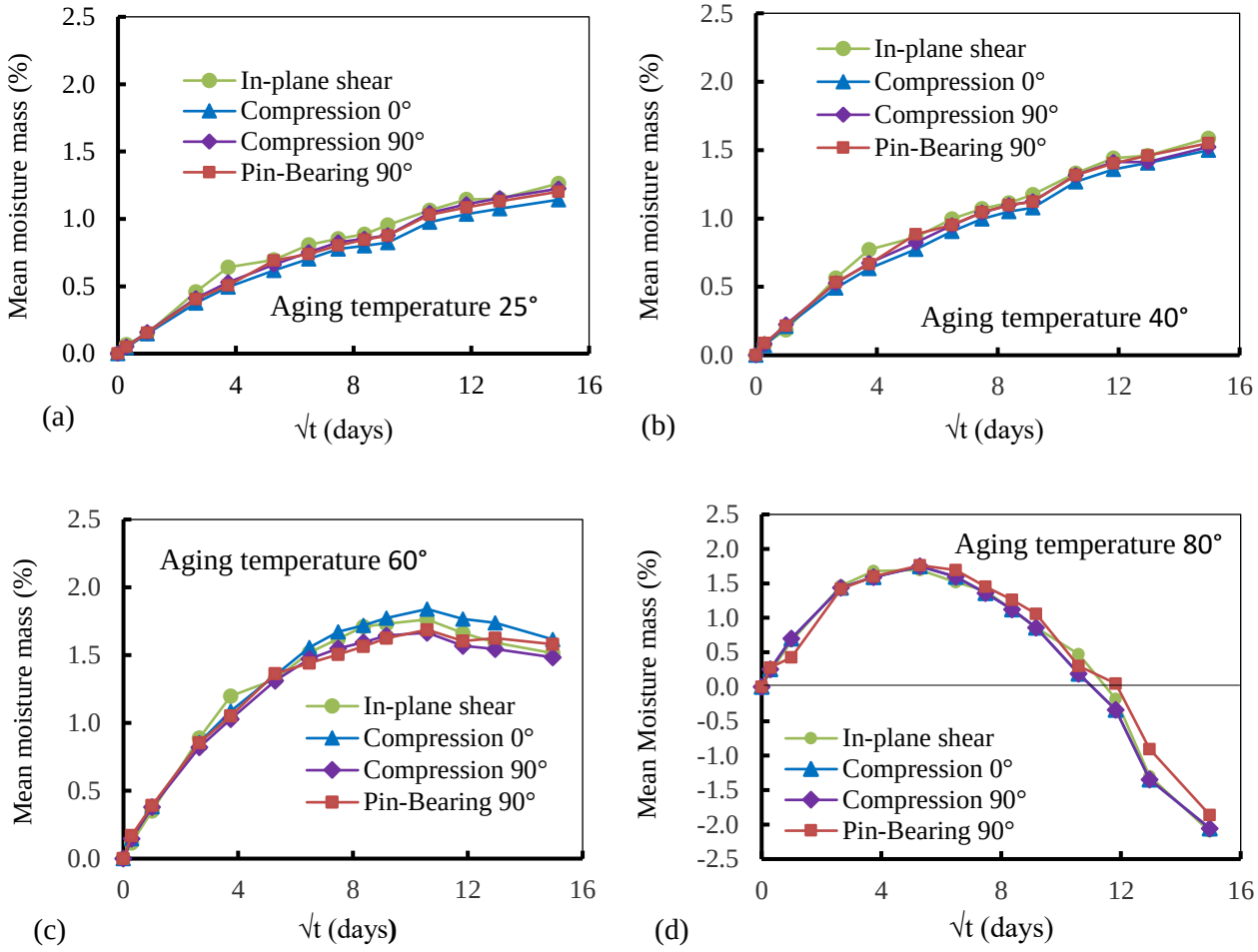

Fig. 5. Mean moisture mass (%) curves against time ($\sqrt{t}$) up to 224 days for three coupon sizes, at the temperature of: (a) 25°C; (b) 40°C; (c) 60°C; (d) 80°C.

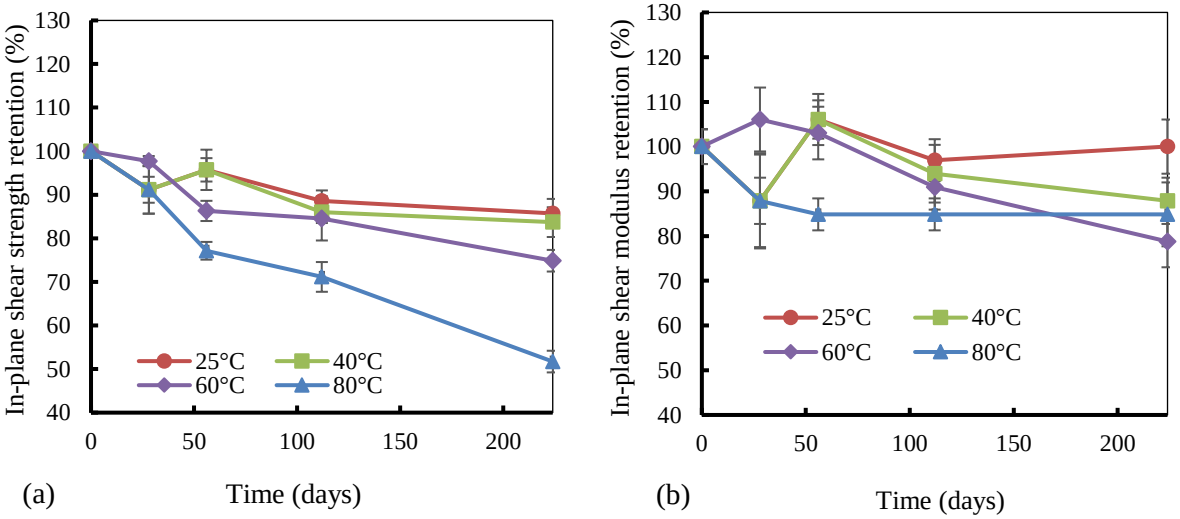

Fig. 6. Test results for "Wet" mean in-plane shear properties with days of aging: (a) Shear strength; (b) Shear modulus.

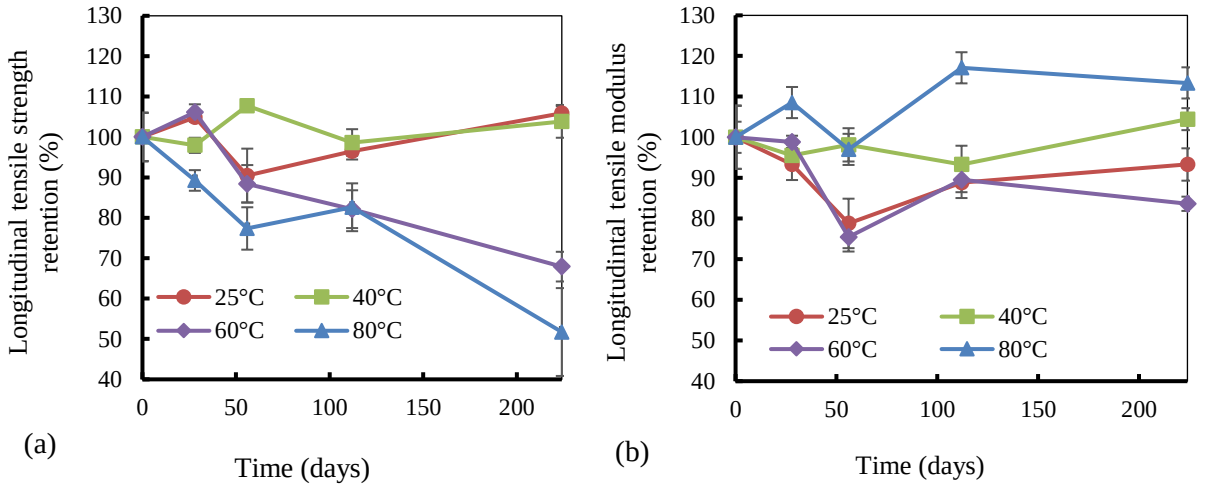

Fig. 7. Test results for "Wet" mean longitudinal tension properties with days of aging: (a) Strength; (b) Modulus of elasticity.

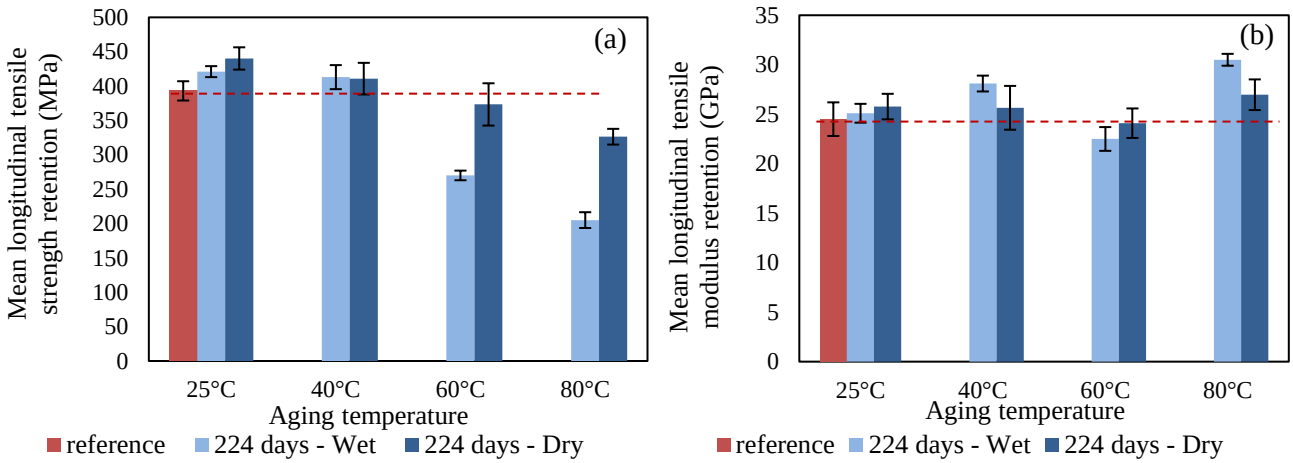

Fig. 8. Bar charts with 'Wet' and 'Dry' coupon test results at 224 days for mean longitudinal tension properties: (a) Strength; (b) Modulus of elasticity.

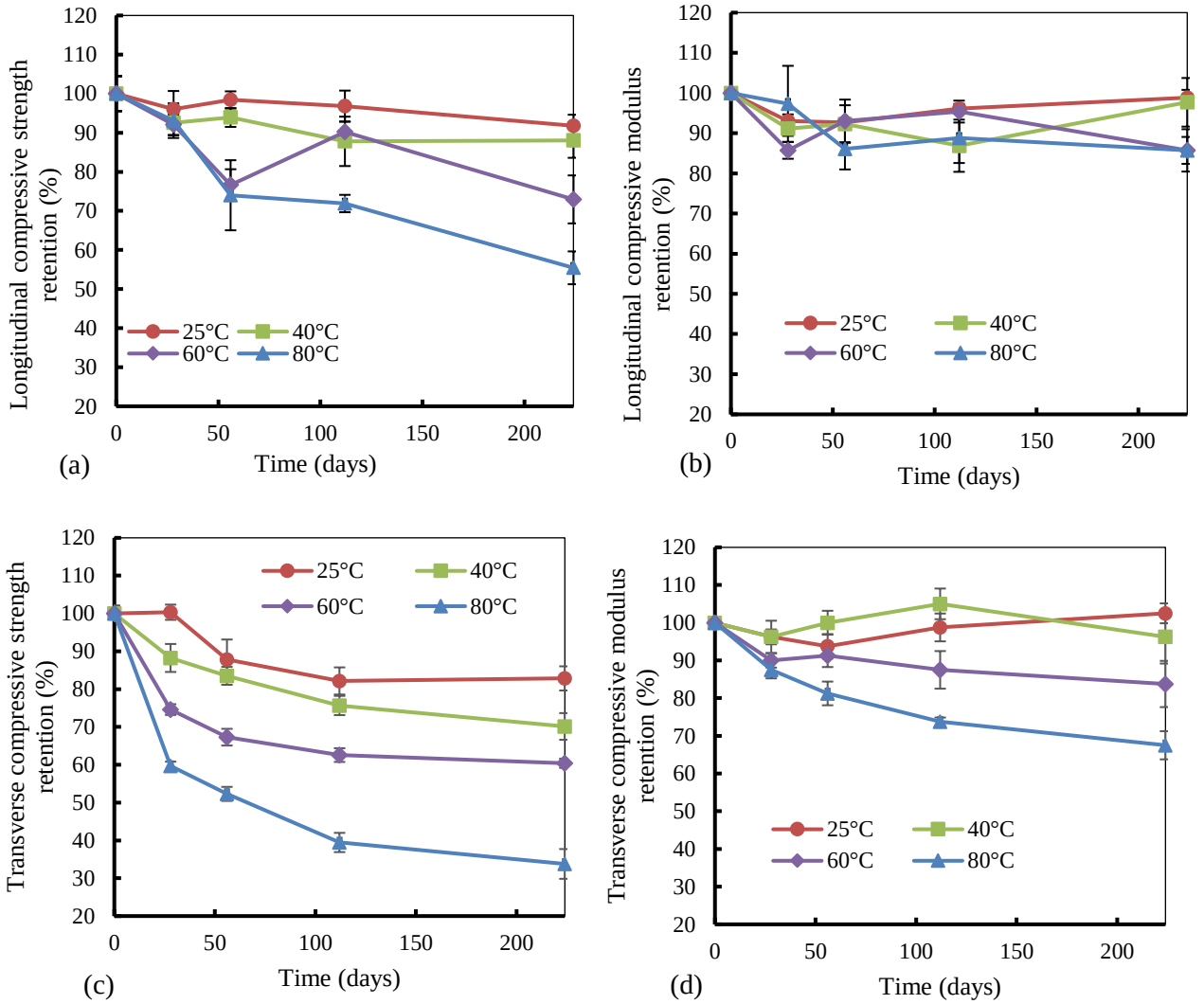

Fig. 9. Test results for "Wet" mean compression properties: (a) Longitudinal strength; (b) Longitudinal modulus of elasticity; (c) Transverse strength; (d) Transverse modulus of elasticity.

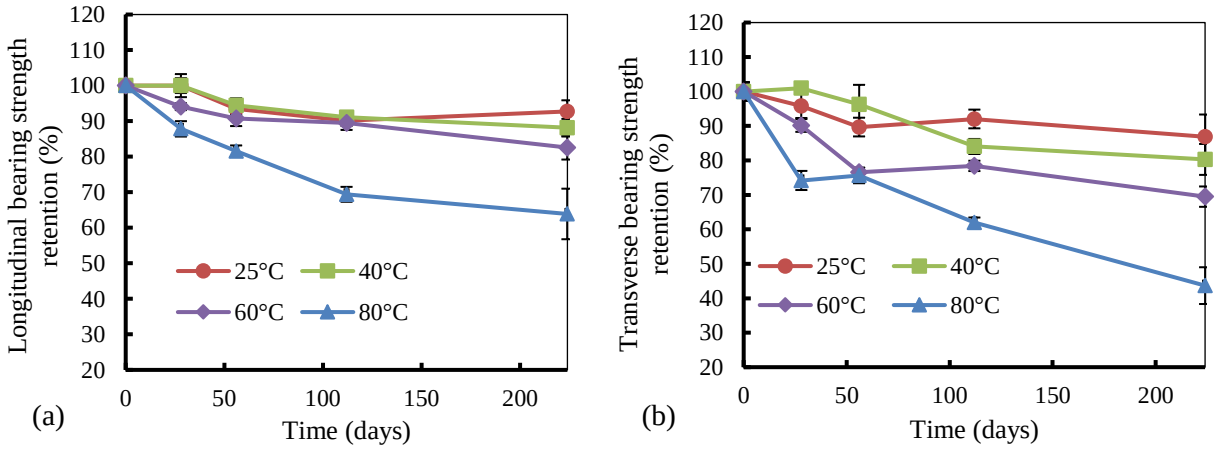

Fig. 10. Test results for "Wet" mean pin-bearing strength: (a) Longitudinal; (b) transverse.

Table 1. Defining coupons, constant aging temperatures and immersion times in days.

Test method (1)	**Coupon side dimensions (mm)** (2)	**Aging temperature (°C)** (3)	**Number of coupons** (4)				
			0 days	28 days	56 days	112 days	224 days
In-plane shear	250 by 25	unaged	5	-	-	-	-
		25	-	5	5	5	5
		40	-	5	5	5	5
		60	-	5	5	5	5
		80	-	5	5	5	5
Tension	250 by 25	unaged	3	-	-	-	-
		25	-	3	3	3	3
		40	-	3	3	3	3
		60	-	3	3	3	3
		80	-	3	3	3	3
Compression	70 by 50	unaged	5×2	-	-	-	-
		25	-	5×2	5×2	5×2	5×2
		40	-	5×2	5×2	5×2	5×2
		60	-	5×2	5×2	5×2	5×2
		80	-	5×2	5×2	5×2	5×2
Pin-bearing	80 by 80	unaged	5×2	-	-	-	-
		25	-	5×2	5×2	5×2	5×2
		40	-	5×2	5×2	5×2	5×2
		60	-	5×2	5×2	5×2	5×2
		80	-	5×2	5×2	5×2	5×2

Table 2. Maximum moisture masses and diffusion coefficients.

Specimen size (mm) (1)	M_∞ (%) (2)				D (10^{-6} mm^2/s) (3)	
	25°C	40°C	60°C	80°C	60°C	80°C
250 by 25	1.26	1.59	1.51	1.69	2.9	8.8
70 by 50 (0°)	1.14	1.50	1.84	1.75	2.9	11.0
70 by 50 (90°)	1.22	1.52	1.67	1.70	2.7	11.1
80 by 80 (90°)	1.20	1.55	1.69	1.76	2.3	6.6

Note: Diffusion coefficients are not determined at 20 or 40°C because after 224 days the specimen had not reach peak mositure saturation.

Table 3. Test results for "Wet" mean in-plane shear strengths and in-plane shear moduli with coefficients of variation (values in backets).

Temperature (1)	Time (days) (2)	τ_{LT} (MPa) (3)	G_{LT} (GPa) (4)
Unaged	0	35 (2)	3.3 (8)
25°C	28	32 (11)	2.9 (21)
	56	34 (9)	3.5 (9)
	112	31 (5)	3.2 (9)
	224	30 (6)	3.3 (11)
40°C	28	32 (11)	2.9 (21)
	56	34 (5)	3.5 (11)
	112	30 (5)	3.1 (12)
	224	29 (7)	2.9 (11)
60°C	28	34 (2)	3.5 (14)
	56	30 (5)	3.4 (11)
	112	30 (10)	2.6 (12)
	224	27 (5)	2.9 (10)
80°C	28	32 (6)	2.9 (10)
	56	27 (4)	2.8 (6)
	112	25 (7)	2.8 (6)
	224	18 (5)	2.8 (13)

1133 Table 4. Test results for mean Longitudinal tensile strengths and Longitudinal tensile modulus of
1134 elasticities with coefficients of variation in percentages (values in backets).

Temperature	Time (days)	$\sigma_{L,t}$ (MPa)		$E_{L,t}$ (GPa)	
		"Dried"	"Wet"	"Dried"	"Wet"
(1)	(2)	(3)	(4)	(5)	(6)
Unaged		393 (7)		24.5 (14)	
25°C	28	385 (6)	417 (2)	24.2 (1)	25.1 (7)
	56	373 (5)	360 (12)	25.2 (4)	21.2 (10)
	112	385 (14)	384 (4)	24.6 (10)	23.9 (7)
	224	440 (7)	421 (6)	25.8 (10)	25.1 (7)
40°C	28	398 (3)	390 (4)	25.2 (1)	25.7 (5)
	56	387 (6)	429 (2)	23.8 (11)	26.4 (8)
	112	387 (15)	393 (6)	24.7 (10)	25.1 (9)
	224	410 (11)	413 (8)	25.6 (17)	28.1 (6)
60°C	28	399 (6)	422 (4)	25.2 (10)	26.6 (10)
	56	406 (4)	352 (8)	24.9 (6)	20.3 (5)
	112	366 (12)	327 (8)	25.0 (9)	24.1 (7)
	224	373 (16)	270 (5)	24.1 (12)	22.5 (10)
80°C	28	300 (7)	355 (5)	24.9 (7)	29.2 (3)
	56	353 (19)	308 (8)	23.3 (13)	26.1 (7)
	112	314 (9)	329 (10)	25.3 (6)	31.5 (7)
	224	326 (7)	206 (11)	27.0 (11)	30.5 (4)

1135

Table 5. Test results for "Wet" mean Longitudinal and Transverse compression strengths and modulus of elasticities with coefficients of variations in percentages (values in backets).

Temperature	Time (days)	Longitudinal compression		Transverse compression	
		$\sigma_{L,c}$ (MPa)	$E_{L,c}$ (GPa)	$\sigma_{T,c}$ (GPa)	$E_{T,c}$ (GPa)
(1)	(2)	(3)	(4)	(5)	(6)
Unaged		377 (9)	25.9 (1)	148 (4)	8.0 (3)
25°C	28	362 (9)	24.1 (3)	149 (4)	7.7 (9)
	56	371 (4)	24.0 (2)	130 (11)	7.5 (6)
	112	365 (8)	24.9 (2)	122 (7)	7.9 (7)
	224	346 (6)	25.6 (4)	123 (6)	8.2 (5)
40°C	28	349 (6)	23.4 (4)	131 (7)	7.7 (4)
	56	354 (5)	23.9 (9)	124 (5)	8.0 (6)
	112	331 (13)	22.5 (13)	112 (5)	8.4 (8)
	224	332 (9)	25.3 (12)	104 (7)	7.7 (14)
60°C	28	347 (5)	22.2 (4)	110 (3)	7.2 (4)
	56	289 (8)	24.1 (11)	100 (4)	7.3 (6)
	112	340 (5)	24.7 (6)	93 (4)	7.0 (10)
	224	275 (12)	22.2 (11)	89 (2)	6.7 (12)
80°C	28	351 (9)	25.2 (19)	88 (2)	7.0 (5)
	56	279 (18)	22.3 (10)	77 (4)	6.5 (6)
	112	271 (4)	23.0 (13)	58 (5)	5.9 (2)
	224	209 (8)	22.2 (7)	50 (8)	5.4 (7)

Table 6. Test results for "Wet" mean Longitudinal and Transvers pin-bearing strengths with coefficients of variation in percentages (values in backets).

Aging temperature	Time (days)	Longitudinal Bearing	Transvers Bearing
		$\sigma_{L,br}$ (MPa)	$\sigma_{T,br}$ (MPa)
(1)	(2)	(3)	(4)
Unaged		304 (3)	213 (5)
25°C	28	304 (4)	204 (7)
	56	284 (3)	191 (5)
	112	274 (3)	196 (5)
	224	282 (6)	185 (13)
40°C	28	304 (6)	215 (3)
	56	287 (4)	205 (11)
	112	277 (3)	179 (4)
	224	268 (5)	171 (9)
60°C	28	286 (2)	192 (4)
	56	276 (4)	163 (3)
	112	272 (4)	167 (3)
	224	251 (7)	148 (6)
80°C	28	267 (4)	158 (6)
	56	248 (3)	161 (4)
	112	211 (4)	132 (3)
	224	194 (14)	93 (11)

1142 Table 7. Data quality stage 1 checks.

Property	$E_{L,c}$	$\sigma_{L,c}$	G_{LT}	τ_{LT}	$E_{T,c}$	$\sigma_{T,c}$	$\sigma_{L,br}$	$\sigma_{T,br}$	$E_{L,t}$	$\sigma_{L,t}$	$\sigma_{L,t}$ ("Dried")
	Table 5		Table 3		Table 5		Table 6		Table 4		
(1)	(2)	(3)	(4)	(5)	(6)	(7)	(8)	(9)	(10)	(11)	(12)
25°C	*1B*	*1A*	*1A, 1B*	*1A*	*1A, 1B*	**X**	*1A*	*1A*	*1A, 1B*	*1A, 1B, 1C*	*1A, 1B, 1C*
40°C	*1A, 1B*	*1A*	*1A*	*1A*	*1A, 1B*	**X**	**X**	**X**	*1A, 1B, 1C*	*1A, 1B, 1C*	*1A, 1B, 1C*
60°C	*1A, 1B*	*1A*	**X**	**X**	*1A*	**X**	**X**	**X**	*1A*	**X**	*1A*
80°C	*1A*	X	*1A*	**X**	X	**X**	*1A*	**X**	*1A, 1B, 1C*	*1A*	*1A, 1B*

1143

1144 Table 8. Data quality Sage 2 checks.

Retention	$E_{L,c}$	$\sigma_{L,c}$	G_{LT}	τ_{LT}	$E_{T,c}$	$\sigma_{T,c}$	$\sigma_{L,br}$	$\sigma_{T,br}$	$E_{L,t}$	$\sigma_{L,t}$	$\sigma_{L,t}$ (dried)
	Table 5		Table 3		Table 5		Table 6		Table 4		
(1)	(2)	(3)	(4)	(5)	(6)	(7)	(8)	(9)	(10)	(11)	(12)
80%	*2B*	**X**	*2B*	**X**	*2A, 2B*	**X**	**X**	**X**	*2A*	*2A, 2B*	*2A, 2B*
70%	*2B*	**X**	*2B*	**X**	*2A, 2B*	**X**	*2A*	**X**	*2A*	*2A, 2B*	*2A, 2B*
60%	*2B*	**X**	*2B*	**X**	*2A, 2B*	**X**	*2A*	**X**	*2A, 2B*	*2A, 2B*	*2A, 2B*
50%	*2B*	**X**	*2B*	**X**	*2A, 2B*	**X**	*2A*	**X**	*2A, 2B*	*2A, 2B*	*2A, 2B*
r^2 (Purnell *et al*. 2008)	-1.0	**0.65**	0.07	**0.74**	0.02	**0.71**	0.54	**0.73**	n/c	n/c	n/c

1145 Note: n/c is for not calculated.

1146 Table 9. Activation energy and statistical data for the Purnell *et al*. (2008) analysis.

Property	Activation energy -E (kJ/mol)	k_0 (day^{-1})	r^2 (Arrhenius)	95% conf. (σ)
(1)	(2)	(3)	(4)	(5)
Longitudinal compressive strength, $\sigma_{L,c}$	45.3	1.50×10^{5}	1.00	0.025
Shear strength, τ_{LT}	30.0	6.67×10^{2}	0.89	0.023
Transverse compressive strength, $\sigma_{T,c}$	56.9	5.92×10^{7}	0.98	0.022
Transverse pin-bearing strength, $\sigma_{T,br}$	43.9	1.67×10^{5}	0.97	0.024

1147

1148 Table 10. Acceleration factors, F, from using Eq. (4).

Service temperature	13°C				18°C			
Ageing temperature	40°C	50°C	60°C	80°C	40°C	50°C	60°C	80°C
$\sigma_{L,c}$	5.2	8.9	15	37	3.7	6.4	11	27
τ_{LT}	3.0	4.2	5.9	11	2.4	3.4	4.8	8.8
$\sigma_{T,c}$	7.9	16	29	94	5.2	10	19	62
$\sigma_{T,br}$	4.9	8.3	14	33	3.6	6.0	10	24

1149

1150 Table 11. Mean service lifetimes ($t_{service}$ in years) at 13°C for each property at various retention levels.

Property	70% Property retention	60%	50%	40%
$\sigma_{L,c}$	11	23	51	129
τ_{LT}	3.9	8.2	18	47
$\sigma_{T,c}$	3.7	7.8	17	44
$\sigma_{T,br}$	5.5	12	26	66

1151